International Journal of Nanomedicine

Dovepress
open access to scientific and medical research

Open Access Full Text Article

ORIGINAL RESEARCH

Green Synthesized Honokiol Transfersomes Relieve the Immunosuppressive and Stem-Like Cell Characteristics of the Aggressive B16F10 Melanoma

Yasmeen Ezzeldeen[1]
Shady Swidan[1,2]
Aliaa ElMeshad[3,4]
Aya Sebak[5]

[1]Department of Pharmaceutics, Faculty of Pharmacy, The British University in Egypt (BUE), El-Sherouk City, Cairo, 11837, Egypt; [2]The Center for Drug Research and Development (CDRD), Faculty of Pharmacy, The British University in Egypt, El-Sherouk City, Cairo, 11837, Egypt; [3]Department of Pharmaceutics and Industrial Pharmacy, Faculty of Pharmacy, Cairo University, Cairo, 11562, Egypt; [4]Department of Bio Nano, Faculty of Nanotechnology for Postgraduate Studies, Cairo University, El-Sheikh Zayed, Giza, 12588, Egypt; [5]Department of Pharmaceutical Technology, Faculty of Pharmacy and Biotechnology, German University in Cairo (GUC), Cairo, Egypt

Background: Honokiol (HK) is a natural bioactive compound with proven antineoplastic properties against melanoma. However, it shows very low bioavailability when administered orally. Alternatively, topical administration may offer a promising route. The objective of the current study was to fabricate HK transfersomes (HKTs) for topical treatment of melanoma. As an ultradeformable carrier system, transfersomes can overcome the physiological barriers to topical treatment of melanoma: the stratum corneum and the anomalous tumor microenvironment. Moreover, the immunomodulatory and stemness-regulation roles of HKTs were the main interest of this study.

Methods: TFs were prepared using the modified scalable heating method. A three-factor, three-level Box–Behnken design was utilized for the optimization of the process and formulation variables. Intracellular uptake and cytotoxicity of HKTs were evaluated in nonactivated and stromal cell–activated B16F10 melanoma cells to investigate the influence of the complex tumor microenvironment on the efficacy of HK. Finally, ELISA and Western blot were performed to evaluate the expression levels of TGF-β and clusters of differentiation (CD47 and CD133, respectively).

Results: The optimized formula exhibited a mean size of 190 nm, highly negative surface charge, high entrapment efficiency, and sustained release profile. HKTs showed potential to alleviate the immunosuppressive characteristics of B16F10 melanoma in vitro via down-regulation of TGF-β signaling. In addition, HKTs reduced expression of the "do not eat me" signal — CD47. Moreover, HKTs possessed additional interesting potential to reduce the expression of the stem-like cell marker CD133. These outcomes were boosted upon combination with metformin, an antihyperglycemic drug recently reported to possess different functions in cancer, while combination with collagenase, an extracellular matrix–depleting enzyme, produced detrimental effects.

Conclusion: HKTs represent a promising scalable formulation for treatment of the aggressive B16F10 melanoma, which is jam-packed with immunosuppressive and stem-like cell markers.

Keywords: honokiol, melanoma, transfersomes, heating method, tumor microenvironment, immunosuppressive, stem-like cell

Correspondence: Shady Swidan
Tel +20 10-0221-1048
Email shady.swidan@bue.edu.eg

Aliaa ElMeshad
Tel +20 10-0010-1551
Email aliaa.elmeshad@pharma.cu.edu.eg

Introduction

Recently, great advances in the field of pharmaceutical biotechnology have been achieved. However, cancer and infectious diseases still occupy the second rank in threats to humanity after cardiovascular diseases. Skin cancer (melanoma)

Received: 8 April 2021
Accepted: 17 June 2021
Published: 24 August 2021

originates from melanin-producing melanocytes, presenting the subtype with the highest mortality and highest potential to metastasize throughout the systemic circulation and lymphatic system traveling to reach distant organs, such as the brain, lungs, and liver.[2–5]

Nowadays, surgical resection is considered the first line of melanoma therapy, in addition to traditional chemotherapy, radiotherapy, immunotherapy, and biological therapy.[6] The failure of most therapeutic agents is due to the immunosuppressive[7–9] and stem-like[10,11] nature of B16F10 melanoma cells, in addition to the complex structure of tumor tissue. The complexity of tumor tissue is due to the tumor microenvironment (TME) which includes a variety of cellular components that contribute to tumor invasion, metastasis, and drug resistance.[12] On one hand, B16F10 melanoma cells exhibit high levels of the "do not eat me" ligand CD47. This is a ligand for SIRPα, an immunoinhibitory receptor, which is expressed on myeloid cells, including macrophages and dendritic cells. The binding of CD47 to SIRPα is a tumor-immunoevasion strategy via inhibition of phagocytosis of tumor cells by immune-system cells.[7–9] In addition, B16F10 melanoma cells express high levels of CD133 (Prom1), which is a membrane glycoprotein characteristic of cancer stem cells (CSCs). CSCs exhibit high potential for tumor growth and metastasis, inhibition of apoptosis, recurrence, and resistance to different therapeutic approaches.[10,11] The key cellular players in the TME are tumor-associated fibroblasts (TAFs) and tumor-associated macrophages (TAMs).[13] TAFs perform multiple activities in tumor formation. They induce the proliferation of tumor tissue contribute to the secretion of collagen and tumor-associated proteins (growth factors), which constitute the dense extracellular matrix (ECM). They also regulate the innate and adaptive immune system by secreting TGF-β, leading to the suppression of antitumor immunoresponses.[14] Furthermore, TAFs contribute to the regulation of polarization of TAMs to their immunosuppressive phenotype M2.[15] This phenotype of TAMs maintains several protumoral functions represented in supporting the progression of tumor growth by increasing the secretion of growth factors and facilitating angiogenesis and metastasis.[16] Various strategies have been employed for TME remodeling, eg, collagenase has been utilized as an ECM-depleting enzyme to digest collagen, facilitating the diffusion of therapeutic agents in tumor tissue.[17–19] Furthermore, metformin, an FDA-approved first-line treatment of type2 diabetes, is currently receiving great attention for its anticancer effects and potential for targeting CSCs.[20] It has been reported that metformin mediates macrophages polarization from the M2 to M1 phenotype[21,22] and possesses a suppressive role on TGF-β signaling.[23–26]

Lately, plant-derived compounds have been proven to have safe pharmacological chemotherapeutic action against various cancer types compared to synthetic chemotherapeutics, with lower toxicity.[27]

A natural bioactive compound derived from species of the Magnoliaceae family(*Magnolia officinalis*, *M. grandiflora*, and *M. obovata*), HK has proven antineoplastic properties against melanoma,[28,29] pancreatic,[30] lung,[31] colorectal,[32] and ovarian cancer,[33] head and neck squamous-cell carcinoma,[34] breast cancer,[35] and even hepatocellular carcinoma.[36] HK has proved to have a lot of striking anticancer activities: it can inhibit angiogenesis, provide direct cytotoxicity, potentiate apoptosis, inhibit multiple-drug resistance, and deregulate cancer cell–signaling pathological pathways involved in growth and malignancy, which it can target.[28,37] HK shows very low oral bioavailability (5%), due to the first-pass effect and low absorption. Alternatively, topical application may offer a promising route, as it is patient-compliant and it can augment HK therapeutic action.[6,38,39] Nevertheless, topical delivery is still challenging, due to the presence of physiological barriers: the stratum corneum, the anomalous TME, and the interstitial matrix.[40,41] Consequently, several nanocarriers have been developed to circumvent the stratum corneum, whereby they can deliver hydrophilic compounds and biomacromolecules to deeper skin layers, achieve a sustained local effect, and enhance topical drug delivery and thus provide high drug bioavailability.[42,43] The structure of transfersomes (TFs) resembles liposomes in composition — both formed of phospholipids — but TFs show superior advantages due to the presence of an edge activator in their composition.[44] An edge activator is a single-chain surfactant that destabilizes the vesicle's phospholipid bilayer and increases its deformability, rendering it an ultradeformable elastic vesicle[45] that can squeeze itself through the intercellular space of the stratum corneum and penetrate deeper skin layers.[44]

Volatile organic solvents like chloroform, ether, or methanol are used in most TF-preparation methods, such as solvent evaporation[46] and thin lipid–film hydration.[47] This leads to the presence of residues of these organic solvents, which may cause toxicity and affect the stability of the final TF preparation. Accordingly, it is advised to avoid the usage of toxic solvents in preparation

procedures.[48,49] This has led to the evolution of the heating method, which can be conducted without the utilization of organic solvents. This method was introduced by Mozafari et al, and involves the application of heat, not lower than the phase-transition temperature (Tc) of the lipids, as below this temperature lipids are present in the gel state and cannot form a closed continuous bilayered structure.[50] The heating method has proved to be a scalable, safe, less time-consuming, and more cost-effective method of nanovesicular preparation.[51] Using drug-delivery systems of these plant-derived compounds formulated by a technique based on green synthesis is an eco-friendly and safe therapeutic modality for human use that can be applied to large-scale production with low cost.[52]

The aim of this study was to follow a green optimized fabrication process of an HK TF–nanodelivery system in order to improve HK bioavailability and skin penetrability. Furthermore, the potential effect on modulating the TME of B16F10 melanoma cells was evaluated in monotherapy or in combination with two TME-remodeling agents — metformin and collagenase — focusing on evaluation of the immunosuppressive and stem-like cell characteristics of B16F10 melanoma cells in response to mono- or combinatorial therapies via evaluation of TGF-β, CD47, and CD133.

Methods

Materials

HK of purity 98% (HPLC) was purchased from Stanford Chemicals, sodium deoxycholate (SDc) from Janssen Pharmaceuticals, soy lecithin and cholesterol from Alfa Aesar, metformin hydrochloride from Sohan Healthcare, and collagenase from Sigma-Aldrich, Germany. Fluorescein isothiocyanate was obtained from Biotium, absolute ethanol from Medico, and HPLC-gradeacetonitrile from Thermo Fisher Scientific. All other chemicals were of analytical grade. Murine melanoma (B16F10, CRL6475), fibroblast (L929, CCL1), and macrophage (RAW264.7, TIB71) cell lines were purchased from the American Type Culture Collection.

Experimental Design

In the present study, three-factor, three-level Box–Behnken design was used to investigate the influence of formulation and process factors and interaction effects on TF characteristics. This design is an optimum approach for ascertaining the effects of formulation/process factors (independent variables) and their associated effects on measured responses (dependent variables).[53] Based on preliminary studies, drug amount (X_1), stirring speed (X_2), and homogenization speed (X_3) were chosen as the independent variables. Particle size (PS;Y_1), PDI (Y_2), Zeta-potential (ZP; Y_3), and drug entrapment efficiency (EE%) (Y_4) were selected as the dependent variables. Table 1 shows the levels of the independent variables and the constraints of the obtained responses/dependent variables. A design matrix comprised of 15 experimental runs with three central points was obtained, as listed in Table 2. After polynomial equations relating the dependent and independent variables had been generated, the process was optimized.

Method of Fabrication

Fifteen TF formulations (Table 2) were fabricated using the modified heating method.[54] Firstly, lecithin (180 mg) and SDc (20 mg) were hydrated individually in 2 mL PBS (pH 7.4) for 1 hour at room temperature, then placed into a preheated mixture of glycerol (3% v/v) and HK (different amounts) at 70°C while stirring at different speeds (1,000, 1,250, and 1,500 rpm) for 1 hour on a hot-plate magnetic stirrer (MSH-20D, 280 V, 50/60 Hz, 660 W, Daihan Scientific). Then, the mixture was left to cool for 30 minutes, leaving the vesicles to anneal and stabilize. Later, the formulations were homogenized using a WiseTis homogenizer (280 W, 50/60 Hz, Daihan Scientific) for 5 minutes, with 60 seconds on and 30 seconds off cycles. Finally, the vesicles were stored in a refrigerator at 4°C for further investigations. The whole fabrication process was performed in a six-baffled homemade vessel (Figure 1) simulating the specially designed glass bottle introduced by Mozafari.[55]

Table 1 Independent and dependent variables of Box–Behnken design utilized to prepare honokiol-loaded transfersome formulations

Independent variables (factors)	**Levels**		
X_1: HK amount (mg)	10	25	40
X_2: Stirring speed (rpm)	1,000	1,250	1,500
X_3: Homogenization speed (rpm)	0	5,000	10,000
Dependent variables (responses)	**Desirability constraints**		
Y_1: Particle size (nm)	Minimize		
Y_2: Polydispersity index	Minimize		
Y_3: Zeta-potential (mV)	Maximize		
Y_4: Entrapment efficiency (%)	Maximize		

Table 2 Experimental runs, independent variables and observed responses of 15 honokiol transfersome formulations prepared according to Box–Behnken design

	X_1 (mg)	X_2 (rpm)	X_3 (rpm)	Y_1 (nm)	Y_2	Y_3 (mV)	Y_4 (%)
HKT1	25	1,000	10,000	213.3±2.86	0.472±0.020	−40.00±0.96	60.00±1.24
HKT2	40	1,000	5,000	306.5±0.64	0.422±0.034	−35.37±1.06	76.24±1.62
HKT3	10	1,000	5,000	475.3±3.82	0.488±0.011	−38.83±1.55	49.46±0.87
HKT4	40	1,250	10,000	139.1±1.85	0.413±0.014	−39.33±1.65	62.60±0.97
HKT5	25	1,250	5,000	234.2±1.02	0.465±0.003	−50.20±2.45	75.00±1.36
HKT6	10	1,250	10,000	131.3±1.54	0.385±0.011	−39.23±1.77	32.60±0.88
HKT7	10	1,250	0	566.8±1.63	0.549±0.011	−44.70±1.22	74.40±1.57
HKT8	40	1,250	0	463.4±1.77	0.435±0.010	−42.50±1.61	89.90±0.96
HKT9	25	1,500	10,000	166.7±0.81	0.444±0.024	−37.47±1.27	76.57±0.47
HKT10	25	1,250	5,000	211.9±3.78	0.469±0.008	−52.93±3.05	77.50±0.99
HKT11	25	1,250	5,000	220.6±1.06	0.48±0.0150	−49.86±2.12	75.75±1.78
HKT12	40	1,500	5,000	314.3±1.87	0.364±0.030	−36.53±0.15	84.38±1.69
HKT13	25	1,500	0	416.2±1.46	0.503±0.011	−44.57±1.52	81.23±0.75
HKT14	10	1,500	5,000	252.20±0.97	0.565±0.007	−43.00±0.34	67.99±0.69
HKT15	25	1,000	0	506.0±2.46	0.588±0.019	−42.93±2.37	84.64±0.73

Notes: X_1, HK amount; X_2, stirring speed; X_3, homogenization speed; Y_1, particle size; Y_2, polydispersity index; Y_3, Zeta potential; Y_4, entrapment efficiency (%).
Abbreviation: HKTs, HK-loaded transfersomes.

Mean Particle Size, Particle-Size Distribution, and ZP

PS and PDI of all formulations were analyzed using a Zetasizer Nano ZS (Malvern Instruments) using dynamic light scattering. ZP was determined from electrophoretic mobility with the same instrument by injecting the samples into a universal folded capillary cell with platinum electrodes at both ends.[56] Freshly prepared TF dispersions were diluted tenfold by deionized water, then PS, PDI, and ZP were measured. Measurements were performed three times and mean PS, PDI, and ZP were calculated.

Determination of HK-Entrapment Efficiency

HK entrapment in the TF vesicles was determined using the indirect method. Briefly, a known volume of the sample was centrifuged at 15,000 rpm for 2 hours at 4°C (Centurion Pro-Research K241R), the supernatant was then separated, and

Figure 1 The six-baffled homemade glass vessel simulating Mozafari's glass bottle.

the absorbance of the free HK was determined with UV-visible spectroscopy (JASCO V-630) at a wavelength with maximum absorbance at 219 nm. EE% was calculated:[57]

$$EE\% = \frac{Total\ HK - Free\ HK\ in\ supernatant}{Total\ HK} \times 100 \quad (1)$$

Optimization of Process Variables

Based on the results obtained, optimization of the variables was conducted using Design-Expert 11 (Stat-Ease) based on the criterion of desirability. The desirability function was introduced by Derringer and Suich.[58] It relies upon the concept that the quality of a novel formulation developed, which has many features, is totally unacceptable if one of the features is outside the desirable limit.[59] The desirability function is used to corroborate compliance with the criteria selected for all involved responses and to provide the best value of compromise in a desirable joint response.[60] This can be achieved by converting the multiple responses evaluated into a single one, combining the individual responses into a composite function, followed by its optimization. To confirm the validity of the optimization process, the suggested HK transfersome (HKT)–optimized formula (HKT_{opt}) with the highest desirability and predicted levels of formulation and process variables was prepared. It was then characterized, and observed values of the responses were compared to the predicted values. The HKT_{opt} formula was then subjected to further investigations.

Transmission Electron Microscopy

The morphology of the HKT_{opt} formula was investigated using transmission electron microscopy (TEM). A drop of the TF suspension was placed on a carbon-coated copper grid and then air-dried at room temperature. The sample was examined at 80 kV with a Hitachi H600.

Deformability Index

For determination of the elasticity of TFs in comparison to liposomes (of relevant composition), the HKT_{opt} and the corresponding liposomal suspension were extruded through a polycarbonate membrane of pore size 50 nm (Thermo Fisher Scientific) applying a constant pressure of 250 kPa (Haug Kompressoren). Deformability-index values were calculated as an indicator of elasticity:[61,62]

$$D = \frac{J}{t(r_v - r_p)^2} \quad (2)$$

where D is the deformability index (mL/second), J the quantity of dispersion extruded (mL), t is the extrusion time (seconds), r_v the vesicle size after extrusion (nm), and r_p the pore size of the extrusion membrane (nm).

Fourier-Transform Infrared Analysis

To assess interactions among HK, lecithin, and SDc, Fourier-transform infrared (FTIR; JASCO FTIR-6200) spectroscopy was performed for these components individually and the HKT_{opt} formula in the 4,000–400 cm^{-1} wavelength range at room temperature with a resolution of 4 cm^{-1}.

In Vitro Release Study

For the determination of HK in vitro release kinetics from TFs, 500 µg HK of the HKT_{opt} and the same amount of free HK in ethanol (1.64 mg/mL) as control were used to compare between the release kinetics of the pure drug and the HKT_{opt}. Each of the HKT_{opt} and the free HK was filled in a dialysis bag made of semipermeable cellulose membrane with molecular weight 12–14 kDa (Spectrum Medical). Each dialysis bag was incubated in a beaker containing a dissolution medium formed of 50 mL 0.5% sodium lauryl sulphate in PBS (pH 7.4 to achieve sink conditions). The whole set was immersed in a shaking water bath (Sci FineTech, 220 V, 50 Hz) at 37°C±1° C and 100 rpm. The experiment was conducted for 24 hours. At predetermined time points, the samples were withdrawn and replaced by an equal volume of the freshly prepared medium. The concentration of the released HK was quantified spectrophotometrically at 219 nm, and the cumulative release profile with time was calculated. This experiment was performed in triplicate.[63]

Establishment of Tumor-Associated Macrophage– and Tumor-Associated Fibroblast–Activated B16F10 Melanoma Culture

For the establishment of TAM-activated and TAF-activated melanoma cultures, B16F10 melanoma cells were cultured in 50% RAW246.7 macrophages or L929 fibroblast-derived conditioned media in fresh culture media for 48 hours. The conditioned media was obtained from confluent cultures of RAW246.7 macrophages or L929 fibroblasts. Successful activation of B16F10 melanoma cells was assessed via evaluation of the concentration of TGF-β from culture supernatants of activated and nonactivated melanoma cells via ELISA. TGF-β secreted by TAMs

and TAFs promotes several hallmarks of tumorigenesis.[64–67]

Intracellular Uptake of Fluorescein-Loaded TFs and Mechanism of Endocytosis

For determination of the intracellular concentration of TFs, a modified protocol by Sebak et al[68] was followed. A noncytotoxic concentration of 250 µg/mL fluorescein-loaded TFs was incubated with the activated and nonactivated B16F10 melanoma cells under 37°C and 5% CO_2. After the predefined incubation of 24 hours, the culture medium containing the noninternalized TFs was discarded. Cells were then washed three times with PBS and fresh media added for the measurement of the fluorescence intensity of the internalized TFs using a multimode microplate reader (Victor 3 V 1420, PerkinElmer) at excitation/emission wavelength of 485/535 nm. A freshly constructed calibration curve of fluorescein-loaded TFs in complete culture medium was utilized for the calculation of the intracellular concentration of TFs.

For determination of the mechanism of endocytic uptake, activated and nonactivated B16F10 melanoma cells were pretreated with endocytic inhibitors in their respective concentrations for 1 hour prior to the addition of the TFs. A 15×10^3 µM quantity of sodium azide, 10^3 µM methyl-β-cyclodextrin (MβCD), and 450 µM sucrose were utilized for evaluation of energy dependence, cholesterol dependence, and clathrin-pit dependence of TF uptake, respectively. Similarly, 20 µM nystatin and 50 µM amiloride were utilized as inhibitors of caveolin-dependent endocytosis and micropinocytosis, respectively.[68–71]

Cytotoxicity of HKTs

For determination of the cytotoxicity of HKTs on activated and nonactivated B16F10 melanoma, a standard MTT assay was used for 1–100 µg/mL of TFs-loaded HK after a predefined incubation time of 24 hours.[72] For determination of the cytotoxicity of the combination therapy, cells were pretreated with the noncytotoxic concentration of metformin (100 µg/mL) or collagenase (50 µg/mL) for 24 hours prior to the addition of HKTs.

Biomarker Analysis

For evaluation of the alteration of different biomarkers in response to the proposed treatment options, activated and nonactivated B16F10 melanoma cells were treated with the half-maximal inhibitory concentration (IC_{50}) of HKTs for 24 hours under standard culture conditions. The biomarkers selected were CD47 and CD133 (in cell lysates), and TGF-β (in the culture supernatant).

Enzyme-Linked Immunosorbent Assay

TGF-β was analyzed from the cell-culture supernatant according to the manufacturer's protocol using a mouse transforming TGF-β ELISA kit (MBS160136) from MyBioSource.

Sodium Dodecyl Sulfate–Polyacrylamide Gel Electrophoresis and Western Blot (WB) Analysis

CD47 and CD133 (Prom1) were analyzed from cell lysates via SDS-PAGE and WB according to the previously published, well-established protocol in the lab of Professor Laila Rashed, Biochemistry Department, Faculty of Medicine, Cairo University.[73,74] CD47 (Thermo Fisher Scientific, 14–0471-82), CD133 (ThermoFisherScientific, 14–1331-82), and β-actin (ThermoFisherScientific, MA1-140) monoclonal antibodies were used for the analysis. Bands for CD47, CD133, and β-actin proteins were visualized by enhanced chemiluminescence (ECL Plus) and quantified relative to β-actin using densitometry and Molecular Analyst software (Bio-Rad).

Statistical Analysis

All experiments were conducted at least three times, and results are expressed as means ± SE. One-way and two-way ANOVA or *t*-test analyses were utilized for statistical evaluation of the data using GraphPad Prism 8.3. Significance was regarded as $P<0.05$. IC_{50} was determined by nonlinear regression analysis of the cytotoxicity data.

Results and Discussion

Analysis of Responses

After fabrication of the 15 HK transfersome (HKT) formulations mentioned in Table 2 by the modified heating method, the impact of the three independent variables — HK amount (X_1), stirring rate (X_2), and homogenization speed (X_3) — on PS (Y_1), PDI (Y_2), ZP (Y_3), and EE% (Y_4) was evaluated using Design Expert 11.

Effect of Process Variables on Particle Size and PDI

Y_1 ranged from 131.3±1.54 nm to 506±2.46 nm, corresponding to HKT6 and HKT15, respectively, as shown in Table 2. Vesicular Y_1 was greatly affected by X_3 ($P<0.0001$)

as speed increased from 0 to 10,000 rpm and decreased sharply from 506±2.46 nm to 131.3±1.54 nm, indicating that homogenization speed was a key parameter in controlling Y_1. Figure 2A shows the response surface plot of the measured Y_1 of the prepared formulations versus X_2 and X_3 respectively. The polynomial equation used relating the particle size to the independent variables was:

$$Y_1 = 222.23 - 25.29X_1 - 43.96X_2 - 162.75X_3 + 57.72X_1X_2 + 27.80X_1X_3 + 10.80X_2X_3 + 57.22X_1 + 57.62X_2 + 45.70X_3 \quad (3)$$

The findings obtained can be explained by the increase inthe mechanical and hydraulic shear as a result of enhancing the homogenization speed, which in turn causes a dramatic decrease in PS.[75] Similar findings were gained by Song et al, who discussed the effect of high-pressure homogenization on the PS of soy protein–isolate suspensions and found reductions in mean PS from 3,331.3 to 146.7 and 135.8 nm after being processed by high-pressure homogenization for 30 passes at 137 and 207 MPa, respectively.[76] Stirring speed produced similar effect on PS whereas smaller PS was obtained at higher stirring speed (1,000-1500).This goes in accordance with previous studies elaborating the effect of stirring speed on surface area[77] and droplet size.[78] As shown in Figure 2A, the lowest PS, 131.3±1.54 nm (HKT6), was achieved at the maximum applied stirring and homogenization speeds — 1,500 and 10,000 rpm, respectively. The results proved that there was no significant effect of drug amount on PS ($P>0.05$), consistent with a study on paromomycin-loaded solid-lipid nanoparticles.[79] Regarding interactions among the independent variables, statistical interpretation of the design coefficients indicated that the combination of both HK amount (X_1) and stirring speed (X_2) had a synergistic effect on particle size of the TF vesicles. The PDI ranged from 0.364±0.030 to 0.588±0.019, represented by HKT12 and HKT15, respectively, as shown in Table 2. The polynomial equation relating PDI (Y_2) to the independent variables can be shown as such:

$$Y2 = 0.4713 - 0.0441X_1 - 0.0118X_2 - 0.0451X_3 - 0.0337X_1X_2 + 0.0355X_1X_3 + 0.0142X_2X_3 - 0.0339X_1 + 0.0223X_2 + 0.0081X_3 \quad (4)$$

The PDI was used as a an indication of size distribution,[80] where a value of 0 was considered as a completely homogeneous system and a value of 1 indicated a highly heterogeneous distribution of vesicles.[81] In reference to Table 2, all samples showed relatively small PDI, indicating their homogeneity and the reliability of all measurements. It was clear

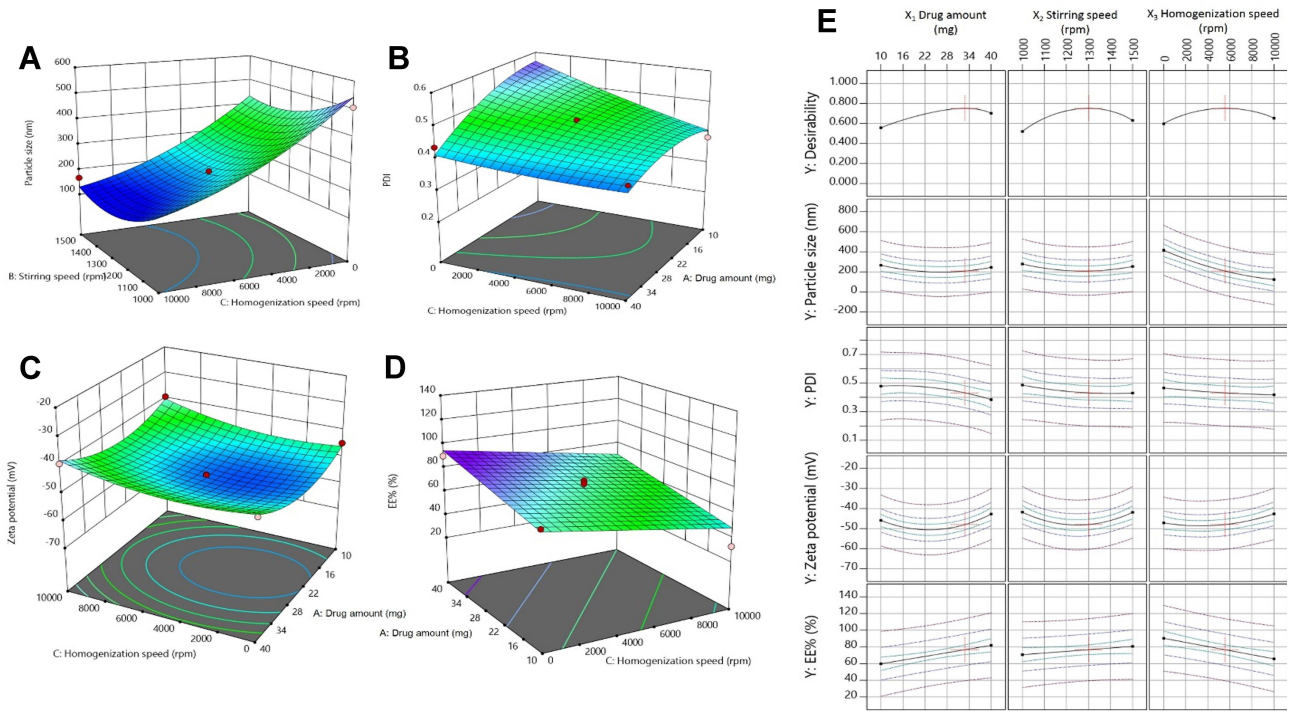

Figure 2 3-D surface response plots showing the relative effects of independent variables on (**A**) particle size, (**B**) PDI, (**C**) Zeta-potential, (**D**) drug EE%, and (**E**) desirability.

that the homogenization speed had a significant impact on particle-size distribution (P=0.0161). The negative of X_3 indicated a negative relationship between homogenization speed and PDI, indicating more uniform size distribution and smaller PDI values with higher homogenization speed. Zidan et al affirmed similar outcomes.[82] It was also found that drug amount had a significant effect on PDI (P=0.0175): its value was diminished by increasing the drug amount, as shown in Figure 2B. It was noticed that good PDI values were obtained in most of the formulations without the use of either sonication or extrusion, the most effective techniques for particle size–distribution reduction. This indicates that the modified heating method is an efficient preparation method that can be scaled up without using expensive organic solvents or energy-consuming processes.

Effect of Variables on ZP

ZP ranged from −35.37±1.06 to −52.93±3.05 mV for HKT2 and HKT10, respectively (Table 2), showing that the TF preparations possessed good stability as ZP >30 mV indicates the stability of the formulations.[56] ZP was significantly affected by homogenization speed (P=0.0184). The polynomial equation relating particle size to the independent variables was:

$$Y3 = -51 + 1.50X_1 - 0.555X_2 + 2.33X_3 + 0.7525X_1X_2 - 0.575X_1X_3 + 1.04X_2X_3 + 6.18X_1 + 6.38X_2 + 3.37X_3 \quad (5)$$

The increase in homogenization speed from 0 to 10,000 rpm resulted in ZP decreasing from −52.93±3.05 to −35.37±1.06 mV, as shown in Figure 2C. This suggests that increasing the energy input in the system led to a decrease in the surface charge. In a study by Severino et al, it was observed that higher homogenization speed led to a reduction in ZP from 24 to 0 mV compromising the dispersion stability and promoting particle agglomeration.[83]

Effect of Process Variables on HK-Entrapment Efficiency

The hydrophobic drug HK was entrapped in lecithin nanovesicles containing SDc as an edge activator. In the experimental design, we kept the quantities of lecithin and SDc fixed and varied the loading amount of HK to determine

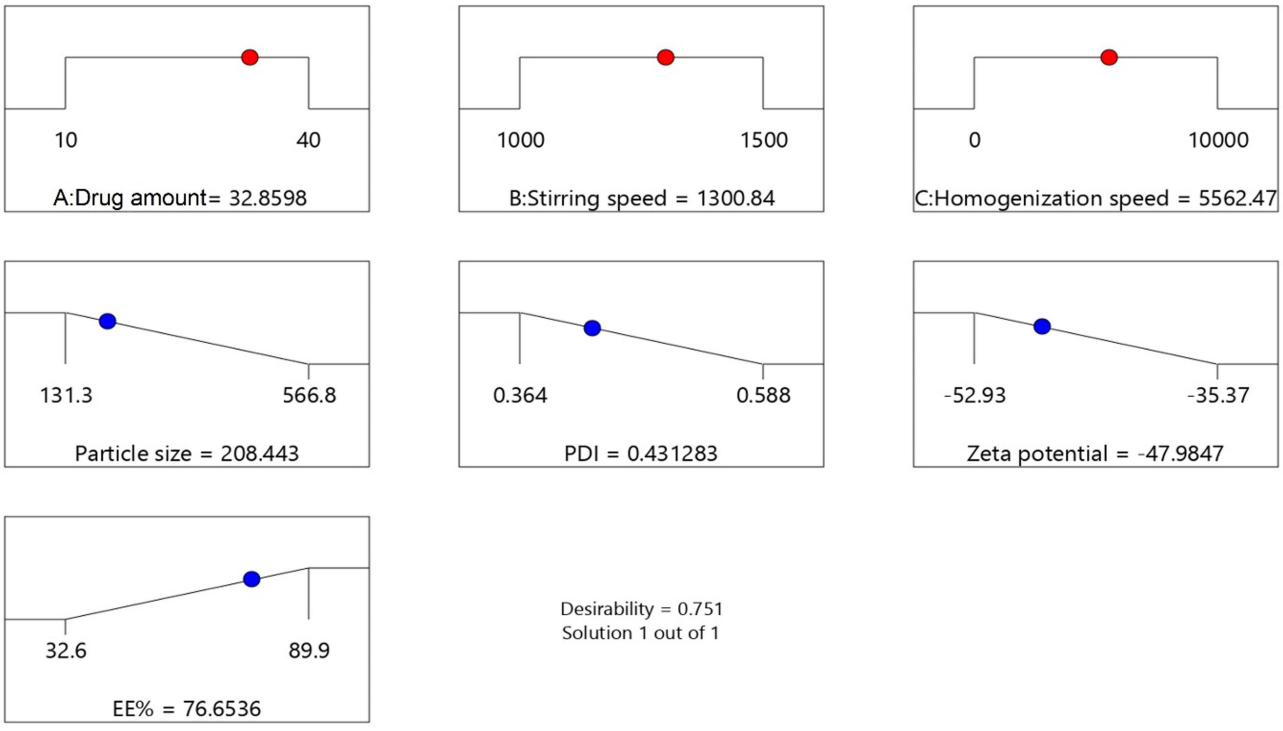

Figure 3 Desirability ramps for the independent variables, with the predicted value of each measured response.

the effect of drug amount on EE%. EE% ranged between 32.6%±0.88% to 89.9%±0.96%, which were the values for HKT6 and HKT8, respectively, as shown in Table 2. Linear regression showed significance (P=0.0008), and the linear model was suggested to best describe the effect of variables on Y_4 as the difference between the adjusted R^2 and predicted R^2 being <0.2. Equation (6) describes the effect of the independent variables on EE%:

$$Y4 = 71.22 + 11.08X_1 + 4.98X_2 - 12.3X_3 \quad (6)$$

Drug amount had a significant effect on HK EE% (P=0.0026). The positive X_1 in the equation indicated that increasing the drug amount resulted in an increase in EE%. Despite that our finding contradicts those observed in a previous study in which the EE% of resveratrol in solid lipid nanoparticles was observed to decrease as drug amount increases.[84] This could be explained on the basis of the hydrophobicity of HK whereas the lipid bilayer represents a better solubilizing vehicle to HK than the external phase composed mainly of PBS (Figure 2D).[85] Statistical analysis also revealed a significant effect of homogenization on drug EE% (P=0.0013), and the negative X_3 indicated an inverse effect of homogenization on EE%. This might be due to the ample shearing effect produced by the application of homogenization that caused disruption of the TF structure, leading to leakage of the drug and thus diminishing drug entrapment.[86] These results are in agreement with a study on Pseudoephedrine HCl loaded nanoliposomes for transdermal delivery.[87] In the current study, the maximum HK EE % (89.9%) was achieved by incorporation of 40 mg of drug in the TFs without the application of homogenization.

Optimization of HKTs Formulation

The aim of the optimization process of HKTs formulation was to determine the levels of the factors studied required to produce a formulation of the highest-possible quality. According to the Box–Behnken model and based on criterion of desirability, the optimum values of the studied variables are suggested in Figure 2E. Desirability-function values range between 0 to 1. The function seeks the most favorable and compromising point in the design space that fulfils the goal for each dependent variable. The suggested values of the independent variables are shown in the optimization ramp (Figure 3). The desirability value of the suggested HKT_{opt} was 0.751.

To confirm the optimization process, the HKT_{opt} was prepared and characterized, then the actual observed responses were compared to the predicted responses of Y_1, Y_2, Y_3, and Y_4 that are listed in Table 3. As seen from the table, there was reasonably good agreement between predicted and observed responses. The adequate predictive performance of the design model justifies its application in the rationalization of an optimal formula and the validity of the optimization design.

TEM of the Optimized HKT Formulation

Morphological examination of HKT_{opt} vesicles was done using TEM, as illustrated in Figure 4. As seen in the figure, it was noted that spherical, well-defined, uniformly sized, and unilamellar vesicles existed as discrete dispersed entities.

Deformability Test

TF vesicles' hallmark is their flexibility compared to liposomes, enabling the TFs to pass easily through the biological membranes.[88] Therefore, the HKT_{opt} was formed of lecithin (the phospholipid) and SDc (the edge activator) at a ratio of 9:1, and its corresponding liposomal suspension consisting of lecithin (the phospholipid) and cholesterol, instead of SDc, at a ratio of 9:1 were selected to be tested for elasticity. The test was conducted by extruding each of the vesicular suspensions through a polycarbonate membrane of pore size 50 nm. The TFs exhibited a higher deformability index (13.9 ±0.9 mL/s) than the liposomes (3.94±1.2 mL/s) according to the deformability index as per equation (2). This is attributed to the presence of the edge activator in the TF structure, which rendered it higher elasticity than liposomes. The deformability index (D-value) of the TF preparation was in strong agreement with a previous study on the preparation of TFs encapsulating sildenafil, which found that the D-value of the best formula containing the optimum phospholipid: surfactant ratio was 14.88 mL/s.[89] Another study done by Salama et al on olanzapine-loaded TFs containing SDc as edge activator showed that a phospholipid:edge-activator molar ratio of 10:1 achieved the highest deformability index in comparison to higher (100:1) or lower (5:1) ratios,

Table 3 Predicted and observed responses of the optimized transfersomal formulation

Independent variables	X_1 (mg)	X_2 (rpm)	X_3 (rpm)
	32.86	1,300	5,562

Response	Y_1 (nm)	Y_2	Y_3 (mV)	Y_4 (%)
Predicted	208.5	0.431	−47.98	76.65
Observed	189.9 ±1.06	0.471 ±0.0001	−53.4 ±1.63	78.92±1.22

as increasing the concentration of SDc in which the phospholipid:SDc molar ratio equaled 5:1 led to diminishing vesicle deformability owing to the steroid-like structure of the SDc, becoming bulkier and resulting in less flexible vesicles.[90]

Fourier-Transform Infrared Analysis

The FTIR spectra of HK, lecithin, SDc, and HKT_{opt} are shown in Figure 5. In the HK spectrum, the peaks in the range of 3,550–3,100 cm^{-1} were due to OH vibration. A band was located at 1,601cm^{-1}, representing the alkene C=C present in HK.[91] The intense bands at 1,495 and 1,426 - cm^{-1} were assigned to the aromatic ring-stretching vibrations of the HK molecule. Other bands were found at 1,205 and 908 cm^{-1} (C–O) and 994 and 824 cm^{-1} (C–C).[92] In lecithin, the broad band centered at 3,318 cm^{-1} was assigned to OH stretching, the principal bands at 2,861 cm^{-1} and 2,927 cm^{-1} corresponding to symmetric and antisymmetric stretching, respectively, in the CH_2 groups of alkyl chains, in addition to the scissoring vibrations at 1,404 cm^{-1} representing the CH_2 groups. The characteristic phosphate-group vibrational band assigned to the PO_2^- antisymmetric stretching mode was centered at 1,232 cm^{-1} and the PO_2^- symmetric stretching mode at 1,083 cm^{-1}.[93] Regarding the SDc spectrum, the three distinctive features at 2,927, 2,861, and 1,556 cm^{-1} are infrared-absorption bands corresponding to CH stretching vibration and COO^- stretching vibration.[94] The FTIR spectra of HKT_{opt} showed that the peaks of the individual samples were shielded or absent and new peaks appeared at 3,268 - cm^{-1} and 1,636 cm^{-1} indicating the occurrence of molecular interactions among the components during TF preparation.

In Vitro Release Study

The release profile (Figure 6) showed that only 50.1% ±2.673% and 53.34%±2.535% of HK was released from the HKT_{opt} after 24 and 48 hours, respectively, in contrast to the ethanolic solution of free drug, which showed 97.629%±3.354% release after 1 hour, indicating the sustained-release effect of the HKT_{opt}. Similar patterns of sustained release were observed for lidocaine, a local anaesthetic, from transferosomes in comparison to the release profile of the free drug.[63]

Extent and Mechanism of Intracellular Uptake of TFs in Nonactivated and TAM- or TAF-Activated Melanoma Cells

The extent of TF accumulation in B16F10 melanoma cells increased upon their incubation with stromal cell–derived conditioned media (Figure 7A). Similar results of higher uptake and retention of nanosystems in activated versus

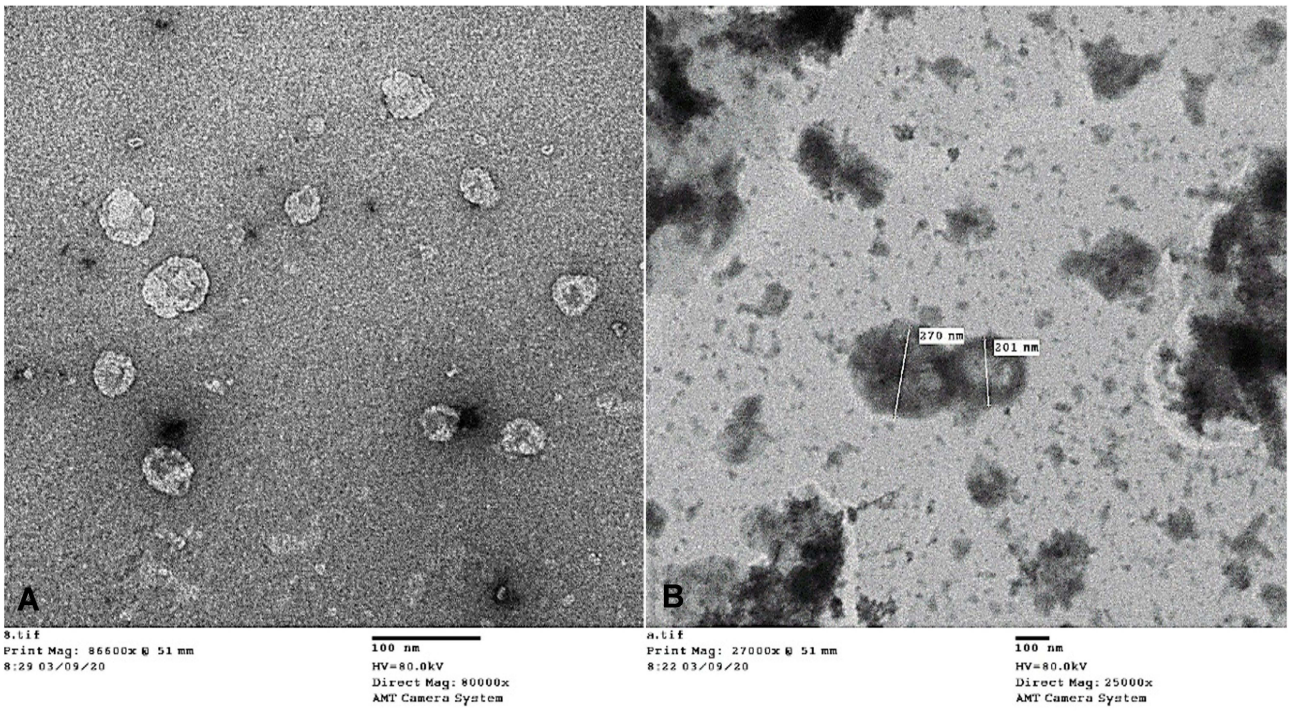

Figure 4 Transmission electron microscopy of the optimized formula at 80 KV, with magnification (**A**) 80,000× and (**B**) 25,000×.

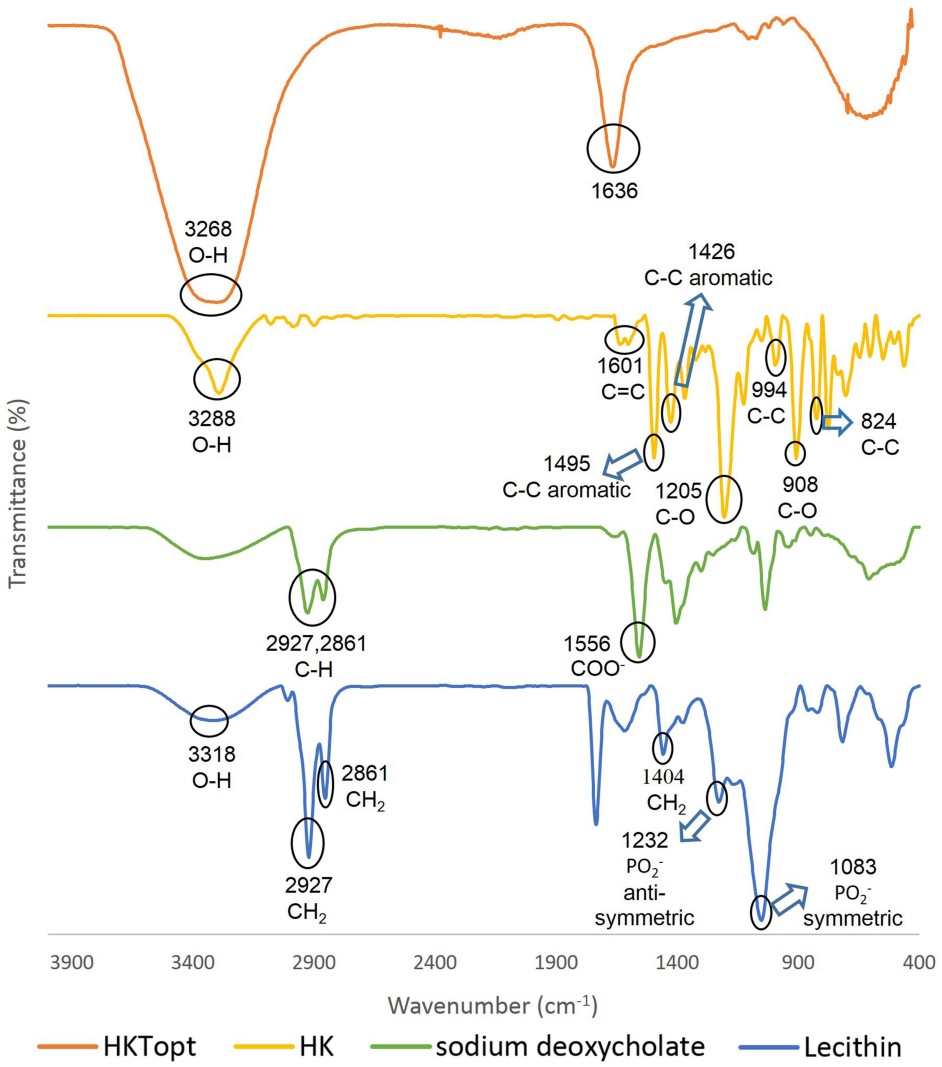

Figure 5 FTIR spectra of pure honokiol, lecithin, sodium deoxycholate, and the optimized formula.

nonactivated cells have been reported for TAFs versus normal fibroblasts[95] and hypoxic versus normoxic phenotypes of breast cancer cells.[96] The variation in the extent of intracellular accumulation of TFs can be explained on the basis of the mechanism of endocytic uptake. Treatment of B16F10 cells with sodium azide, an ATP-depleting agent, prior to the incubation of TFs caused a reduction in the extent of their accumulation, especially in nonactivated and TAF-activated cells (Figure 7B and D, respectively) suggesting the involvement of energy-dependent pathways in TFs uptake.[68] Similarly, amiloride, which inhibits macropinocytosis,[70] caused a very significant reduction in TF cellular concentration levels. Nystatin, which inhibits caveolin-dependent endocytosis,[71] did not result in a significant change in intracellular concentration of the TFs. Regarding the involvement of cholesterol-dependent endocytosis, as suggested from the effect of pretreatment with MβCD, a reduction in TF intracellular uptake was observed in both nonactivated and TAF-activated cells (Figure 7B and D, respectively). Surprisingly, the extent of TF intracellular uptake increased in the case of TAM-activated cells (Figure 7C) upon utilization of MβCD and sucrose, which inhibit cholesterol-dependent[68] and clathrin-dependent[97] endocytosis, respectively. This suggests that blocking one endocytic mechanism could facilitate the uptake of TFs via an alternative pathway, which could be more efficient and/or more rapid.[98]

Cytotoxicity of HKTs in Activated and Nonactivated Melanoma Cells

The effect of HKTs on the viability of B16F10 melanoma cells when cultured in fresh medium or conditioned medium

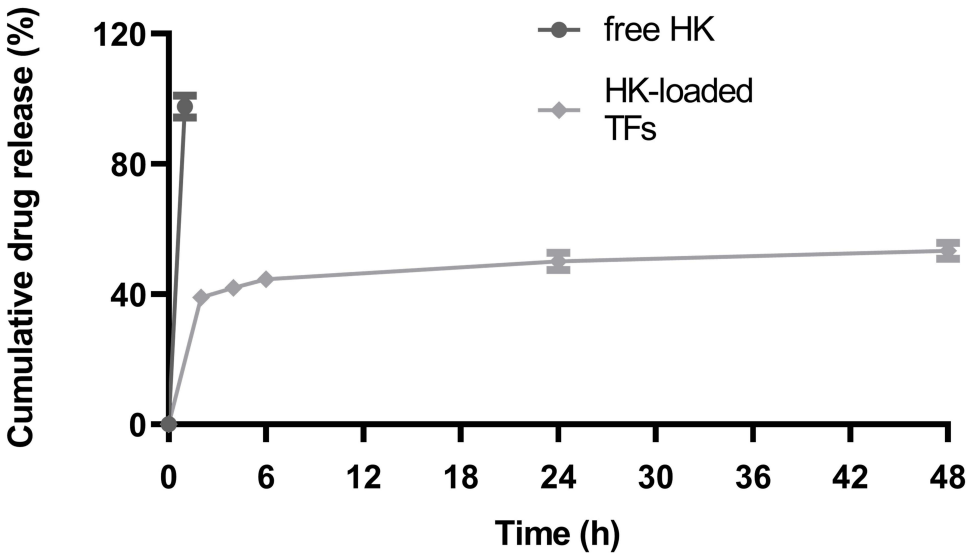

Figure 6 In vitro release profile of honokiol, showing the cumulative percentage released from the optimized formula in PBS (pH 7.4) and the ethanolic solution of the pure form (n=3).

derived from a culture of RAW264.7 macrophages and L929 fibroblasts was assessed. HK has been previously reported to possess appealing anticancer effects in hepatocellular carcinoma,[99] triple-negative breast cancer,[100] hepatoma,[101] oral squamous-cell carcinoma,[102] lung,[103] thyroid,[104] and ovarian cancer,[105] and osteosarcoma.[106] Upon activation of melanoma cells with conditioned media derived from stromal-cell cultures, a significant increase in IC_{50} was observed (Figure 8). This contradicts the observed increase in the concentration of TFs in activated melanoma cells. This could be attributed to the development of resistance mechanisms upon induction of cell–cell interactions when cells were incubated with cytokine-rich conditioned media, as could be observed from the levels of TGF-β in TAM- and TAF-activated melanoma cells (Figure 10). TGF-β is a potent protumorigenic and immunosuppressive cytokine that regulates multiple functions in the TME.[64–67]

Intracellular Uptake and Cytotoxicity of TFs upon Pretreatment with TME-Remodeling Agents (Metformin and Collagenase)

Pretreatment with either metformin or collagenase did not result in any contribution to the extent of the intracellular accumulation of the TFs in nonactivated or TAF-activated B16F10 melanoma cells (Figure 9A). However, collagenase pretreatment significantly increased the intracellular concentration of TFs in TAM-activated B16F10 melanoma cells. This could be explained by the ability of collagenase to digest dense ECM components, eg, collagen which could have facilitated uptake of the TFs. Enhancement in the uptake of magnetic nanoparticles in pancreatic cancer cells has been reported with pretreatment with collagenase.[107] A similar observation was recorded for permeability of nanoparticles in 3-D spheroids.[18]

Unexpectedly,the susceptibility of nonactivated melanoma cells to HK-mediated cytotoxicity decreased significantly upon pretreatment with collagenase (Figure 9B). However, this could be explained on the basis of the ability of collagenase to increase TGF-β activation,[108] consistent with our results elaborated in Figure 10, which has multiple implications in cancer resistance to different chemotherapeutics.[109] On the contrary, metformin and collagenase pretreatment were shown to increase the efficacy of HKTs in TAM- and TAF-activated melanoma (Figure 9C and D, respectively), pointing to a possible synergistic effect whereas both agents previously showed multiple roles in the TME.[17–26]

Role of HKTs on Immunosuppressive and Stem-Like Cell Characteristics of B16F10 Melanoma Cells in Monotherapy or Combined with TME-Remodeling Agents (Metformin and Collagenase)

TAM- and TAF-activated melanoma cells exhibited higher levels of all the immunosuppressive (TGFβ and CD47) and stem-like cell (CD133) markers relative to

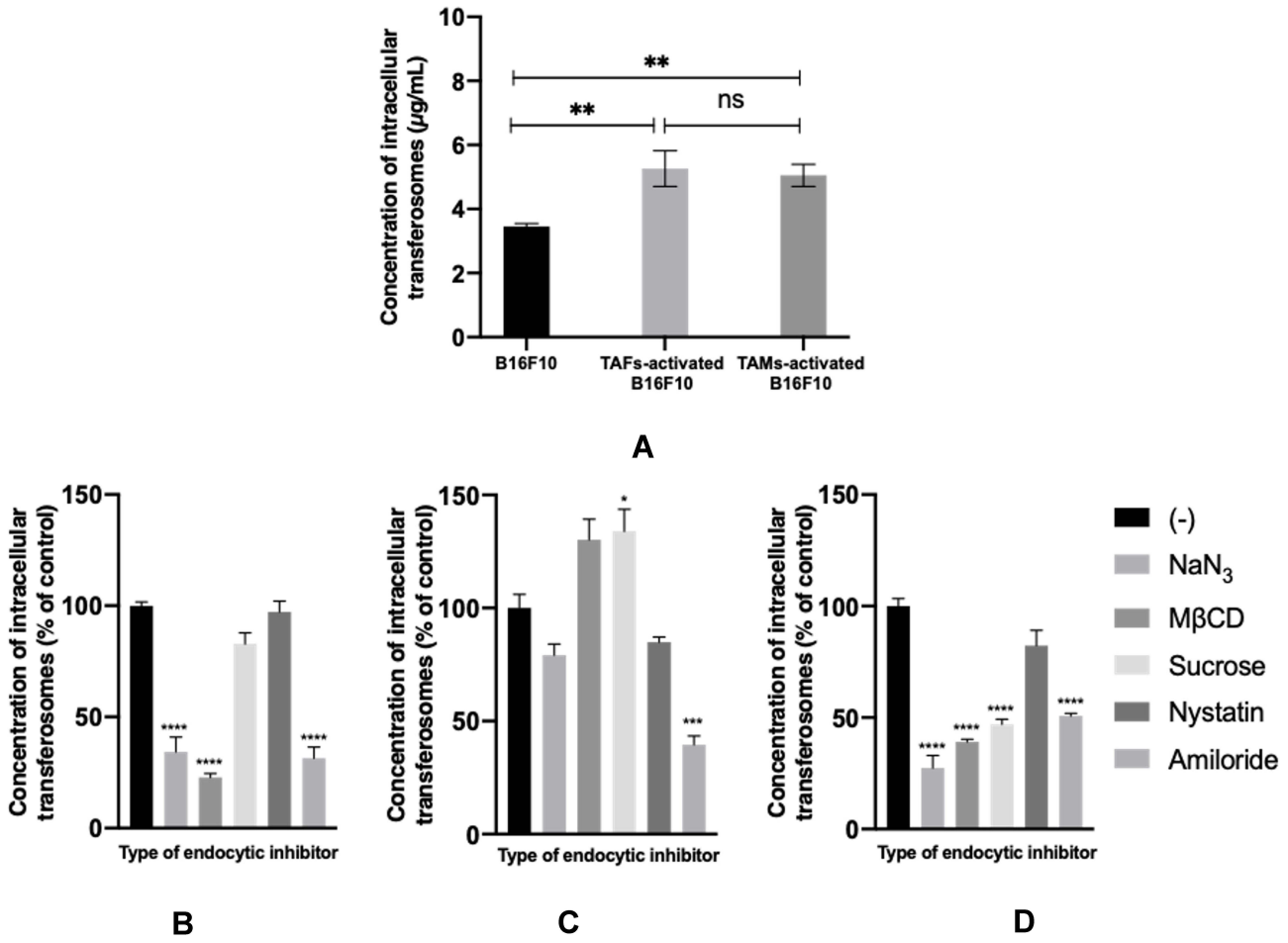

Figure 7 Intracellular uptake of fluorescein-loaded TFs in nonactivated and TAM- or TAF-activated B16F10 melanoma cells (**A**). Mechanism of endocytic uptake of TFs in nonactivated (**B**), TAM-activated (**C**), and TAF-activated (**D**) B16F10 melanoma cells. ns, not significant. *p<0.05; **p<0.01; **p<0.001; ****p<0.0001.

nonactivated melanoma cells (Figure 10A and B, respectively). It is well known that TGF-β can be secreted from tumor cells, TAMs,[64,65] and TAFs,[66,67] promoting proliferation, angiogenesis, immunosuppression, ECM remodeling, invasion, and metastasis.[111–115] In addition, TGF-β has been reported to regulate cancer stemness and induce the expression of stem-like cell markers like CD133.[115–117] CSCs can then secrete more TGF-β, regulating all immunohallmarks in the tumor, including the expression of CD47.[118] This shows how the TME is highly orchestrated and that all the three markers are interrelated.

Treatment of TAM-activated cells with HKTs reduce the levels of TGF-β, CD47, and CD133 (Figure 10A and Figure S1A–C). This could be explained on the basis of the previously reported role of HK in exhibiting an immunogenic effect in gastric cancer via inducing endoplasmic reticulum stress, blocking epithelial–mesenchymal transition, and suppressing calreticulin.[119] A prophagocytic marker associated with poor prognosis of some cancer types, calreticulin has been positively correlated with the antiphagocytic CD47 for maintaining cellular homeostasis by balancing pro- and antiphagocytic signals.[120] Therefore, the suppressive effect observed for HK in our study on CD47 could have been regulated indirectly via calreticulin. Another possible explanation for the reduced levels of CD47 in HK-treated cells is the downregulation of TGF-β signaling: CD47 expression has been previously reported to be associated with TGF-β expression.[121] Moreover, HK possesses CSC-targeting potential, reduces the proliferation of $CD133^{+}$ CSCs, and reverts the conferred resistance to chemotherapy in glioblastoma multiforme and oral squamous- cell carcinoma.[122–124]

Further improvement in the therapeutic outcome of TAM-activated melanoma cells was observed upon pretreatment with metformin. Metformin has been reported

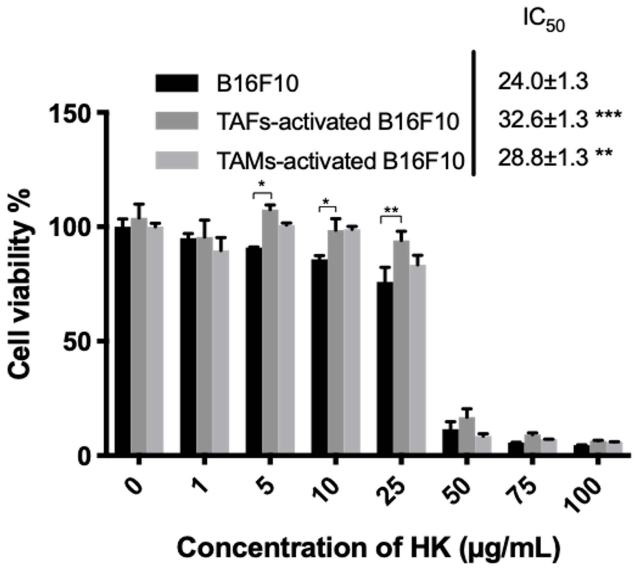

Figure 8 Cytotoxicity of HKTs in activated and nonactivated B16F10 melanoma cells. *p<0.05; *; p<0.01; ***; p<0.001.

to reduce TGF-β expression and attenuate TGFβ-mediated tumorigenesis.[26] It also possesses a repressing role on tumor initiation, self-renewal, and chemoresistance conferred by the breast cancer stem cells (BCSCs). Metformin was found to cause miR-708 mediated repression of the gene CD47 facilitating phagocytosis of BCSCs by macrophages.[125] Metformin also mediates the downregulation of CD133 in hepatocellular carcinoma[126] and pancreatic cancer,[127,128] affecting higher chemosensitivity.

In an opposite manner, pretreatment of TAM-activated melanoma cells with collagenase produced an undesirable impact. This could be explained by the previously reported anti-inflammatory role of collagenase: it was found to upregulate anti-inflammatory cytokines, IL10, and TGF-β and downregulate the proinflammatory cytokines TNFα and IL1β.[129]

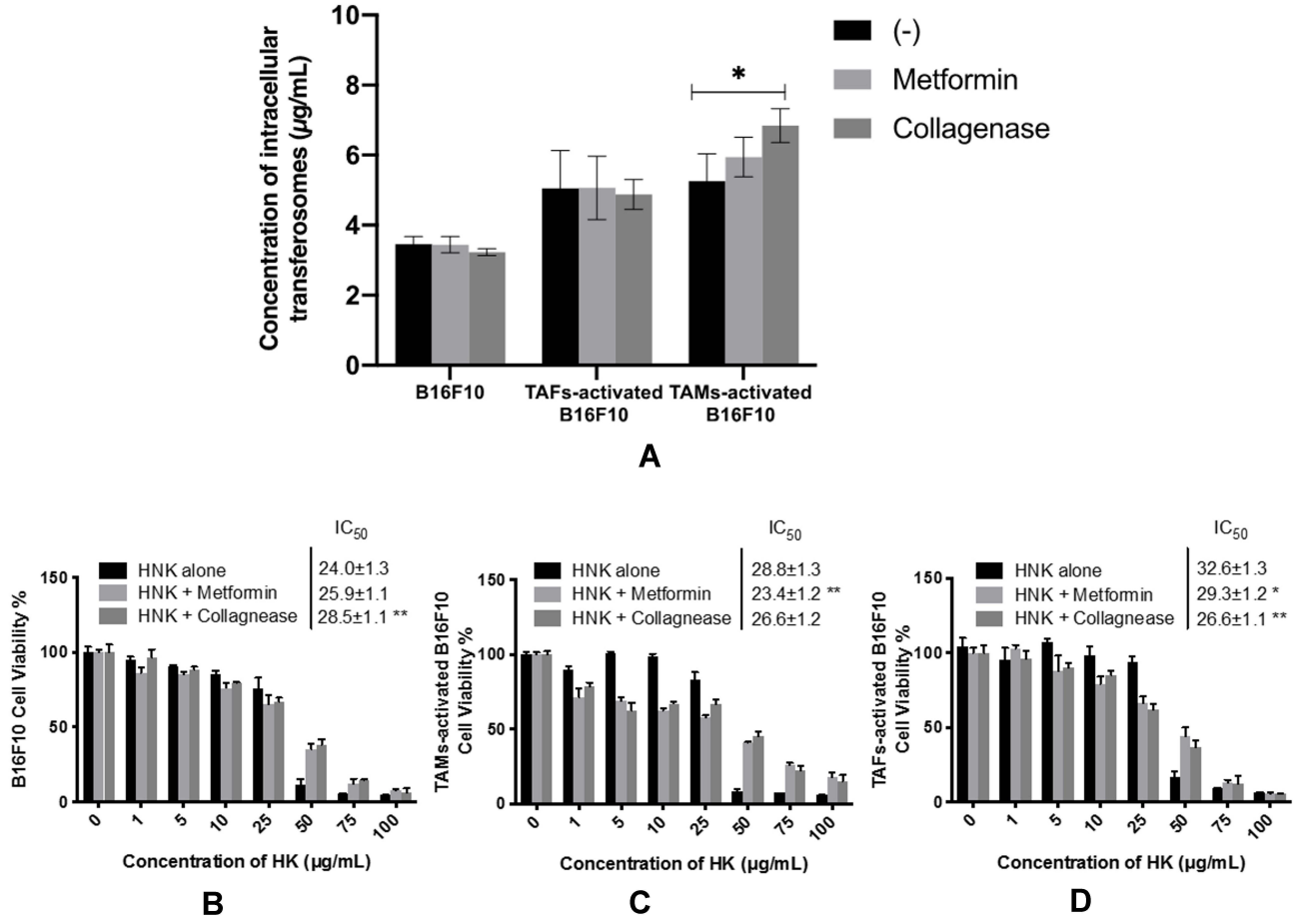

Figure 9 Intracellular uptake of fluorescein-loaded TFs in nonactivated and TAM- or TAF-activated melanoma cells upon combination with TME remodeling agents (metformin and collagenase) (**A**). Cytotoxicity of HKTs in nonactivated (**B**), TAM-activated (**C**), and TAF-activated (**D**) B16F10 melanoma cells upon combination with TME remodeling agents (metformin and collagenase). *P<0.05; *; p<0.01.

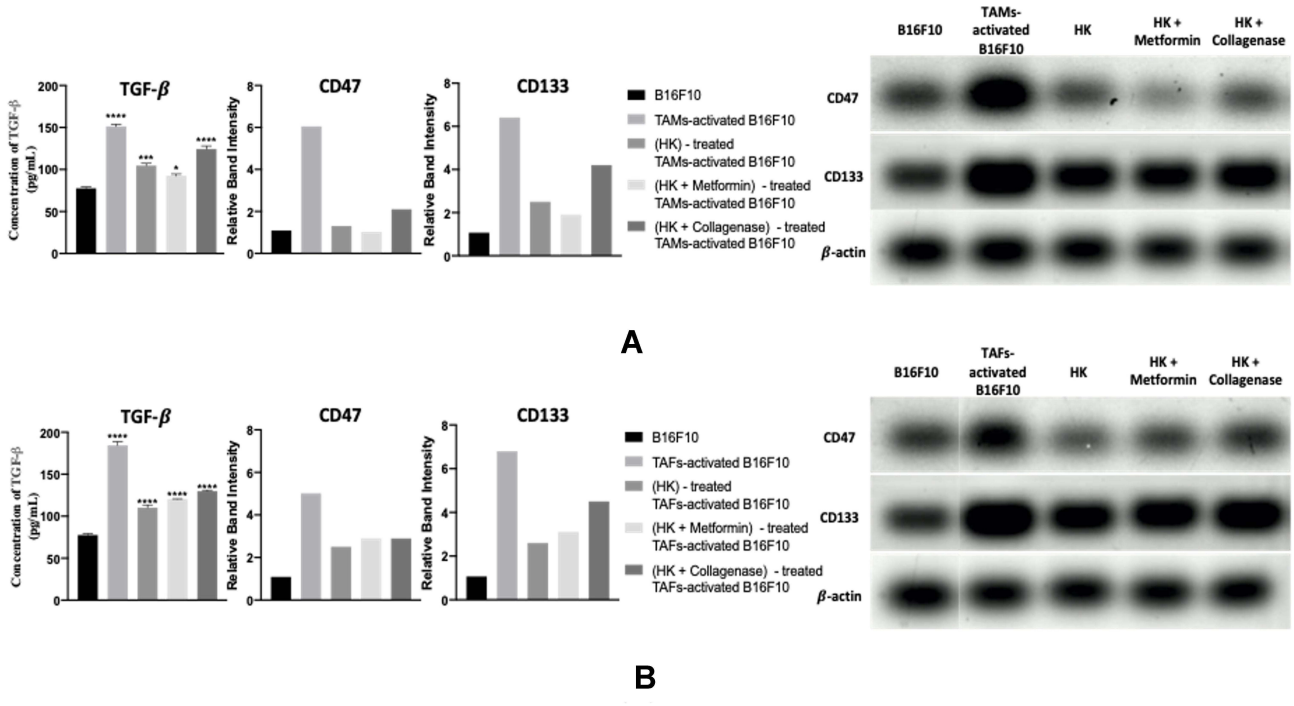

Figure 10 Role of HKTs on the immunosuppressive (TGFβ and CD47) and stem-like cell (CD133) markers of TAM-activated (**A**) and TAF-activated (**B**) B16F10 melanoma cells. TGF-β concentration was analyzed with ELISA, while CD47 and CD133 were analyzed with WB. Bands for CD47, CD133, and β-actin proteins were visualized by enhanced chemiluminescence (ECL Plus) and quantified relative to β-actin using densitometry and Molecular Analyst Software. Uncropped blots of CD47, CD133, and β-actin proteins are provided in the supplementary materials (Figure S1A–C, respectively). *p<0.05; *****p<0.001; **p<0.0001.

Treatment of TAF-activated cells with HKTs reduced levels of all the tested markers (Figure 10B and Figure S1A–C). However, the combination therapy produced detrimental effects on the level of the immunosuppressive and stem-like cell characteristics of melanoma. While the effect of collagenase pretreatment was not surprising, the detrimental effect of metformin was not expected. Investigation of the literature for a possible explanation revealed tha metformin has a positive role on the secretion of TGF-β in supernatants of 4T1 triple-negative breast cancer cells.[130]

Conclusion

Atoxic HKTs were successfully fabricated using a simple, scalable, green, modified heating method. Box–Behnken surface analysis proved to be an efficient tool to optimize the HKT formulations. HKTs possessed uniform nanosize, high negative charge, high EE%, and sufficient elasticity, and provided sustained release of HK over 48 hours. Moreover, HKTs reduce levels of TGF-β, CD47, and CD133, alleviating the immunosuppressive and stem-like cell characteristics of melanoma cells. Further improvement in therapeutic outcome was observed upon pretreatment with metformin, while pretreatment with collagenase produced an undesirable effect. With the view that the TME is highly orchestrated, it is necessary to investigate the role of the proposed topical HKT therapy on other key players of the TME.

Acknowledgment

We would like to thank Professor Laila Rashed, Professor of Medical Biochemistry and Molecular Biology, Cairo University for helping with the ELISA and WB experiments.

Disclosure

The authors reported no conflicts of interest for this work.

References

1. Khorrami S, Zarrabi A, Khaleghi M, Danaei M, Mozafari MR. Selective cytotoxicity of green synthesized silver nanoparticles against the MCF-7 tumor cell line and their enhanced antioxidant and antimicrobial properties. *Int J Nanomedicine.* 2018:8013-8024. doi:10.1016/j.pdpdt.2017.01.186.
2. Gomaa I, Sebak A, Afifi N, Abdel-Kader M. Liposomal delivery of ferrous chlorophyllin: a novel third generation photosensitizer for in vitro PDT of melanoma. *Photodiagnosis Photodyn Ther.* 2017;18:162–170. doi:10.1016/j.pdpdt.2017.01.186
3. Sebak AA, Gomaa II, ElMeshad AN, AbdelKader MH. Targeted photodynamic-induced singlet oxygen production by peptide-conjugated biodegradable nanoparticles for treatment of skin melanoma. *Photodiagnosis Photodyn Ther.* 2018;23:181–189. doi:10.1016/j.pdpdt.2018.05.017

4. Rady M, Gomaa I, Afifi N, Abdel-Kader M. Dermal delivery of Fe-chlorophyllin via ultradeformable nanovesicles for photodynamic therapy in melanoma animal model. *Int J Pharm*. 2018;548(1):480–490. doi:10.1016/j.ijpharm.2018.06.057
5. Tran MA, Watts RJ, Robertson GP. Use of liposomes as drug delivery vehicles for treatment of melanoma. *Pigment Cell Melanoma Res*. 2009;22(4):388–399. doi:10.1111/j.1755-148X.2009.00581.x
6. Jiang T, Wang T, Li T, et al. Enhanced transdermal drug delivery by transfersome-embedded oligopeptide hydrogel for topical chemotherapy of melanoma. *ACS Nano*. 2018;12(10):9693–9701. doi:10.1021/acsnano.8b03800
7. Schwartz AL, Nath PR, Allgauer M, et al. Antisense targeting of CD47 enhances human cytotoxic T-cell activity and increases survival of mice bearing B16 melanoma when combined with anti-CTLA4 and tumor irradiation. *Cancer Immunol Immunother*. 2019;68(11):1805–1817. doi:10.1007/s00262-019-02397-7
8. Sockolosky JT, Dougan M, Ingram JR, et al. Durable antitumor responses to CD47 blockade require adaptive immune stimulation. *Proc Natl Acad Sci U S A*. 2016;113(19):E2646–E2654. doi:10.1073/pnas.1604268113
9. Li Y, Zhang M, Wang X, Liu W, Wang H, Yang YG. Vaccination with CD47 deficient tumor cells elicits an antitumor immune response in mice. *Nat Commun*. 2020;11(1):1–11. doi:10.1038/s41467-019-14102-4
10. Kumar D, Kumar S, Gorain M, et al. Notch1-MAPK signaling axis regulates CD133+ cancer stem cell-mediated melanoma growth and angiogenesis. *J Invest Dermatol*. 2016;136(12):2462–2474. doi:10.1016/j.jid.2016.07.024
11. Blancas-Mosqueda M, Zapata-Benavides P, Zamora-ávila D, et al. CD133 antisense suppresses cancer cell growth and increases sensitivity to cisplatin in vitro. *Exp Ther Med*. 2012;4(5):901–905. doi:10.3892/etm.2012.692
12. Chen B, Dai W, Mei D, et al. Comprehensively priming the tumor microenvironment by cancer-associated fibroblast-targeted liposomes for combined therapy with cancer cell-targeted chemotherapeutic drug delivery system. *J Control Release*. 2016;241:68–80. doi:10.1016/j.jconrel.2016.09.014
13. Hu K, Miao L, Goodwin TJ, Li J, Liu Q, Huang L. Quercetin remodels the tumor microenvironment to improve the permeation, retention, and antitumor effects of nanoparticles. *ACS Nano*. 2017;11(5):4916–4925. doi:10.1021/acsnano.7b01522
14. Ohshio Y, Hanaoka J, Kontani K, Teramoto K. Tranilast inhibits the function of cancer-associated fibroblasts responsible for the induction of immune suppressor cell types. *Scand J Immunol*. 2014;80(6):408–416. doi:10.1111/sji.12242
15. Kamata T, So TY, Ahmed Q, et al. Fibroblast-derived STC-1 modulates tumor-associated macrophages and lung adenocarcinoma development. *Cell Rep*. 2020;31(12):107802. doi:10.1016/j.celrep.2020.107802
16. Mantovani A, Schioppa T, Porta C, Allavena P, Sica A. Role of tumor-associated macrophages in tumor progression and invasion. *Cancer Metastasis Rev*. 2006;25(3):315–322. doi:10.1007/s10555-006-9001-7
17. Zinger A, Koren L, Adir O, et al. Collagenase nanoparticles enhance the penetration of drugs into pancreatic tumors. *ACS Nano*. 2019;13(10):11008–11021. doi:10.1021/acsnano.9b02395
18. Goodman TT, Olive PL, Pun SH. Increased nanoparticle penetration in collagenase-treated multicellular spheroids. *Int J Nanomedicine*. 2007;2(2):265–274.
19. Lee S, Han H, Koo H, et al. Extracellular matrix remodeling in vivo for enhancing tumor-targeting efficiency of nanoparticle drug carriers using the pulsed high intensity focused ultrasound. *J Control Release*. 2017;263:68–78. doi:10.1016/j.jconrel.2017.02.035
20. Lei Y, Yi Y, Liu Y, et al. Metformin targets multiple signaling pathways in cancer. *Chin J Cancer*. 2017;36(1):1–9. doi:10.1186/s40880-017-0184-9
21. Ding L, Liang G, Yao Z, et al. Metformin prevents cancer metastasis by inhibiting M2-like polarization of tumor associated macrophages. *Oncotarget*. 2015;6(34):36441–36455. doi:10.18632/oncotarget.5541
22. Wang J-C, Sun X, Ma Q, et al. Metformin's antitumour and anti-angiogenic activities are mediated by skewing macrophage polarization. *J Cell Mol Med*. 2018;22(8):3825–3836. doi:10.1111/jcmm.13655
23. Luo T, Nocon A, Fry J, et al. AMPK activation by metformin suppresses abnormal extracellular matrix remodeling in adipose tissue and ameliorates insulin resistance in obesity. *Diabetes*. 2016;65(8):2295–2310. doi:10.2337/db15-1122
24. Cheng K, Hao M. Metformin inhibits TGF-β1-induced Epithelial-to-mesenchymal transition via PKM2 relative-mTOR/p70s6k signaling pathway in cervical carcinoma cells. *Int J Mol Sci*. 2016;17(12):2000. doi:10.3390/ijms17122000
25. Xiao H, Zhang J, Xu Z, et al. Metformin is a novel suppressor for transforming growth factor (TGF)-β1. *Sci Rep*. 2016;6. doi:10.1038/srep28597
26. Wahdan-Alaswad R, Harrell JC, Fan Z, Edgerton SM, Liu B, Thor AD. Metformin attenuates transforming growth factor beta (TGF-β) mediated oncogenesis in mesenchymal stem-like/claudin-low triple negative breast cancer. *Cell Cycle*. 2016;15(8):1046–1059. doi:10.1080/15384101.2016.1152432
27. Yeruva L, Elegbede JA, Carper SW. Methyl jasmonate decreases membrane fluidity and induces apoptosis through tumor necrosis factor receptor 1 in breast cancer cells. *Anticancer Drugs*. 2008;19(8):766–776. doi:10.1097/CAD.0b013e32830b5894
28. Arora S, Singh S, Piazza GA, Contreras CM, Panyam J, Singh AP. Honokiol: a novel natural agent for cancer prevention and therapy. *Curr Mol Med*. 2012;12(10):1244–1252. doi:10.2174/156652412803833508
29. Guillermo-Lagae R, Santha S, Thomas M, et al. Antineoplastic effects of honokiol on melanoma. *Biomed Res Int*. 2017;2017:1–10. doi:10.1155/2017/5496398
30. Arora S, Bhardwaj A, Srivastava SK, et al. Honokiol arrests cell cycle, induces apoptosis, and potentiates the cytotoxic effect of gemcitabine in human pancreatic cancer cells. *PLoS One*. 2011;6(6):e21573. doi:10.1371/journal.pone.0021573
31. Jiang QQ, Fan LY, Yang GL, et al. Improved therapeutic effectiveness by combining liposomal honokiol with cisplatin in lung cancer model. *BMC Cancer*. 2008;8(1):1–8. doi:10.1186/1471-2407-8-242
32. Chen F, Wang T, Wu YF, et al. Honokiol: a potent chemotherapy candidate for human colorectal carcinoma. *World J Gastroenterol*. 2004;10(23):3459–3463. doi:10.3748/wjg.v10.i23.3459
33. Liu Y, Chen L, He X, et al. Enhancement of therapeutic effectiveness by combining liposomal honokiol with cisplatin in ovarian carcinoma. *Int J Gynecol Cancer*. 2008;18(4):652–659. doi:10.1111/j.1525-1438.2007.01070.x
34. Leeman-Neill RJ, Cai Q, Joyce SC, et al. Honokiol inhibits epidermal growth factor receptor signaling and enhances the antitumor effects of epidermal growth factor receptor inhibitors. *Clin Cancer Res*. 2010;16(9):2571–2579. doi:10.1158/1078-0432.CCR-10-0333
35. Nagalingam A, Arbiser JL, Bonner MY, Saxena NK, Sharma D. Erratum to: honokiol activates AMP-activated protein kinase in breast cancer cells via LKB1-dependent pathway and inhibits breast carcinogenesis. *Breast Cancer Res*. 2017;19(1):39. doi:10.1186/s13058-017-0829-2
36. Yang J, Pei H, Luo H, et al. Non-toxic dose of liposomal honokiol suppresses metastasis of hepatocellular carcinoma through destabilizing EGFR and inhibiting the downstream pathways. *Oncotarget*. 2017;8(1):915–932. doi:10.18632/oncotarget.13687

37. Ahn KS, Sethi G, Shishodia S, Sung B, Arbiser JL, Aggarwal BB. Honokiol potentiates apoptosis, suppresses osteoclastogenesis, and inhibits invasion through modulation of nuclear factor-κB activation pathway. *Mol Cancer Res*. 2006;4(9):621–633. doi:10.1158/1541-7786.MCR-06-0076
38. Puig L, Carrascosa JM, Belinchón I, et al. Adherence and patient satisfaction with topical treatment in psoriasis, and the use, and organoleptic properties of such treatments: a delphi study with an expert panel and members of the psoriasis group of the spanish academy of dermatology and venereolo. *Actas Dermosifiliogr*. 2013;104(6):488–496. doi:10.1016/j.adengl.2012.12.003
39. Lin CF, Hwang TL, Al-Suwayeh SA, Huang YL, Hung YY, Fang JY. Maximizing dermal targeting and minimizing transdermal penetration by magnolol/honokiol methoxylation. *Int J Pharm*. 2013;445(1–2):153–162. doi:10.1016/j.ijpharm.2013.01.049
40. Sandilands A, Sutherland C, Irvine AD, McLean WHI. Filaggrin in the frontline: role in skin barrier function and disease. *J Cell Sci*. 2009;122(9):1285–1294. doi:10.1242/jcs.033969
41. Jain RK, Stylianopoulos T. Delivering nanomedicine to solid tumors. *Nat Rev Clin Oncol*. 2010;7(11):653–664. doi:10.1038/nrclinonc.2010.139
42. Neubert RHH. Potentials of new nanocarriers for dermal and transdermal drug delivery. *Eur J Pharm Biopharm*. 2011;77(1):1–2. doi:10.1016/j.ejpb.2010.11.003
43. Fernández-garcía R, Lalatsa A, Statts L, Bolás-fernández F. Transferosomes as nanocarriers for drugs across the skin: quality by design from lab to industrial scale. *Int J Pharm*. 2020;573(July 2019):118817. doi:10.1016/j.ijpharm.2019.118817
44. El ZGM, Awad GAS, Holayel SM, Mortada ND. Role of edge activators and surface charge in developing ultradeformable vesicles with enhanced skin delivery. *Int J Pharm*. 2010;397(1–2):164–172. doi:10.1016/j.ijpharm.2010.06.034
45. Kumar A, Nayak A, Ghatuary SK. Design, Optimization and Characterization of a Transferosomal Gel of Acyclovir for Effective Treatment of Herpes Zoster. *J. Drug Deliv. Ther*. 2019;9:712–721. doi:10.22270/jddt.v9i4-A.3556.
46. Ezzat SM, Salama MM, ElMeshad AN, Teaima MH, Rashad LA. HPLC–DAD–MS/MS profiling of standardized rosemary extract and enhancement of its anti-wrinkle activity by encapsulation in elastic nanovesicles. *Arch Pharm Res*. 2016;39(7):912–925. doi:10.1007/s12272-016-0744-6
47. Qushawy M, Nasr A, Abd-Alhaseeb M, Swidan S. Design, optimization and characterization of a transfersomal gel using miconazole nitrate for the treatment of candida skin infections. *Pharmaceutics*. 2018;10(1):26. doi:10.3390/pharmaceutics10010026
48. Panahi Y, Farshbaf M, Mohammadhosseini M, et al. Recent advances on liposomal nanoparticles: synthesis, characterization and biomedical applications. *Artif Cells Nanomed Biotechnol*. 2017;45(4):788–799. doi:10.1080/21691401.2017.1282496
49. Mortazavi SM, Mohammadabadi MR, Khosravi-Darani K, Mozafari MR. Preparation of liposomal gene therapy vectors by a scalable method without using volatile solvents or detergents. *J Biotechnol*. 2007;129(4):604–613. doi:10.1016/j.jbiotec.2007.02.005
50. Mozafari MR. Liposomes: an overview of manfacturing techniques. *Cell Mol Biol Lett*. 2005;10:37–47.
51. Jahadi M, Khosravi-Darani K, Ehsani MR, Mozafari MR, Saboury AA, Pourhosseini PS. The encapsulation of flavourzyme in nanoliposome by heating method. *J Food Sci Technol*. 2015;52(4):2063–2072. doi:10.1007/s13197-013-1243-0
52. Rajan R, Chandran K, Harper SL, Yun S-I, Kalaichelvan PT. Plant extract synthesized silver nanoparticles: an ongoing source of novel biocompatible materials. *Ind Crops Prod*. 2015;70:356–373. doi:10.1016/j.indcrop.2015.03.015
53. Yadav P, Rastogi V, Verma A. Application of Box–Behnken design and desirability function in the development and optimization of self-nanoemulsifying drug delivery system for enhanced dissolution of ezetimibe. *Future J Pharm Sci*. 2020;6(1). doi:10.1186/s43094-020-00023-3
54. Elmeshad AN, Mortazavi SM, Mozafari MR. Formulation and characterization of nanoliposomal 5-fluorouracil for cancer nanotherapy. *J Liposome Res*. 2014;24(1):1–9. doi:10.3109/08982104.2013.810644
55. Colas J-C, Shi W, Rao VSNM, Omri A, Mozafari MR, Singh H. Microscopical investigations of nisin-loaded nanoliposomes prepared by Mozafari method and their bacterial targeting. *Micron*. 2007;38(8):841–847. doi:10.1016/j.micron.2007.06.013
56. Das S, Ng WK, Kanaujia P, Kim S, Tan RBH. Formulation design, preparation and physicochemical characterizations of solid lipid nanoparticles containing a hydrophobic drug: effects of process variables. *Colloids Surf B*. 2011;88(1):483–489. doi:10.1016/j.colsurfb.2011.07.036
57. Nasr S, Rady M, Gomaa I, et al. Ethosomes and lipid-coated chitosan nanocarriers for skin delivery of a chlorophyll derivative: a potential treatment of squamous cell carcinoma by photodynamic therapy. *Int J Pharm*. 2019;568:118528. doi:10.1016/j.ijpharm.2019.118528
58. Derringer G, Suich R. Simultaneous Optimization of Several Response Variables. *J Qual Technol*. 1980;12(4):214–219. doi:10.1080/00224065.1980.11980968
59. Nasr AM, Elhady SS, Swidan SA, Badawi NM. Celecoxib loaded in-situ provesicular powder and its in-vitro cytotoxic effect for cancer therapy: fabrication, characterization, optimization and pharmacokinetic evaluation. *Pharmaceutics*. 2020;12(12):1–20. doi:10.3390/pharmaceutics12121157
60. Vera Candioti L, De Zan MM, Cámara MS, Goicoechea HC. Experimental design and multiple response optimization. Using the desirability function in analytical methods development. *Talanta*. 2014;124:123–138. doi:10.1016/j.talanta.2014.01.034
61. Kaur IP, Rana C, Singh M, Bhushan S, Singh H, Kakkar S. Development and evaluation of novel surfactant-based elastic vesicular system for ocular delivery of fluconazole. *J Ocul Pharmacol Ther*. 2012;28(5):484–496. doi:10.1089/jop.2011.0176
62. Elazreg R, Soliman M, Mansour S, El Shamy A. Preparation and evaluation of mucoadhesive gellan gum in-situ gels for the ocular delivery of carbonic anhydrase inhibitor nanovesicles. *Int J Pharm Sci Res*. 2015;6(9):3761–3774. doi:10.13040/IJPSR.0975-8232.6(9).3761-74
63. Bnyan R, Khan I, Ehtezazi T, et al. Formulation and optimisation of novel transfersomes for sustained release of local anaesthetic. *J Pharm Pharmacol*. 2019;71(10):1508–1519. doi:10.1111/jphp.13149
64. Cai J, Xia L, Li J, Ni S, Song H, Wu X. Tumor-associated macrophages derived TGF-β-induced epithelial to mesenchymal transition in colorectal cancer cells through Smad2,3–4/Snail signaling pathway. *Cancer Res Treat*. 2019;51(1):252–256. doi:10.4143/crt.2017.613
65. Zhang D, Qiu X, Li J, Zheng S, Li L, Zhao HTGF-B. secreted by tumor-associated macrophages promotes proliferation and invasion of colorectal cancer via miR-34a-VEGF axis. *Cell Cycle*. 2018;17(24):2766–2778. doi:10.1080/15384101.2018.1556064
66. Sun DY, Wu JQ, He ZH, He MF, Bin SH. Cancer-associated fibroblast regulate proliferation and migration of prostate cancer cells through TGF-β signaling pathway. *Life Sci*. 2019;235:116791. doi:10.1016/j.lfs.2019.116791
67. Siljamäki E, Rappu P, Riihilä P, Nissinen L, Kähäri VM, Heino J. H-Ras activation and fibroblast-induced TGF-β signaling promote laminin-332 accumulation and invasion in cutaneous squamous cell carcinoma. *Matrix Biol*. 2020;87:26–47. doi:10.1016/j.matbio.2019.09.001

68. Sebak A, Gomaa I, ElMeshad A, et al. Distinct proteins in protein corona of nanoparticles represent a promising venue for endogenous targeting part i: in vitro release and uptake perspective. *Int J Nanomedicine*. 2020;2020(15):8845–8862. doi:10.2147/IJN.S273713
69. Tang H, Chen H, Jia Y, et al. Effect of inhibitors of endocytosis and NF-kB signal pathway on folate-conjugated nanoparticle endocytosis by rat Kupffer cells. *Int J Nanomedicine*. 2017;12:6937–6947. doi:10.2147/IJN.S141407
70. Thompson DB, Villaseñor R, Dorr BM, Zerial M, Liu DR. Cellular uptake mechanisms and endosomal trafficking of supercharged proteins. *Chem Biol*. 2012;19(7):831–843. doi:10.1016/j.chembiol.2012.06.014
71. Li Y, Monteiro-Riviere NA. Mechanisms of cell uptake, inflammatory potential and protein corona effects with gold nanoparticles. *Nanomedicine*. 2016;11(24):3185–3203. doi:10.2217/nnm-2016-0303
72. Bahuguna A, Khan I, Bajpai VK, Kang SC. MTT assay to evaluate the cytotoxic potential of a drug. *Bangladesh J Pharmacol*. 2017;12(2):115–118. doi:10.3329/bjp.v12i2.30892
73. Youness RA, Hafez HM, Khallaf E, Assal RA, Abdel Motaal A, Gad MZ. The long noncoding RNA sONE represses triple-negative breast cancer aggressiveness through inducing the expression of miR-34a, miR-15a, miR-16, and let-7a. *J Cell Physiol*. 2019;234(11):20286–20297. doi:10.1002/jcp.28629
74. Hashem RM, Rashed LA, Hassanin KMA, Hetta MH, Ahmed AO. Effect of 6-gingerol on AMPK- NF-κB axis in high fat diet fed rats. *Biomed Pharmacother*. 2017;88:293–301. doi:10.1016/j.biopha.2017.01.035
75. Maleki Dizaj S, Lotfipour F, Barzegar-Jalali M, Zarrintan MH, Adibkia K. Application of Box–Behnken design to prepare gentamicin-loaded calcium carbonate nanoparticles. *Artif Cells Nanomed Biotechnol*. 2016;44(6):1475–1481. doi:10.3109/21691401.2015.1042108
76. Song X, Zhou C, Fu F, Chen Z, Wu Q. Effect of high-pressure homogenization on particle size and film properties of soy protein isolate. *Ind Crops Prod*. 2013;43(1):538–544. doi:10.1016/j.indcrop.2012.08.005
77. Yasir M, Sara UVS. Preparation and optimization of haloperidol loaded solid lipid nanoparticles by Box–Behnken design. *J Pharm Res*. 2013;7(6):551–558. doi:10.1016/j.jopr.2013.05.022
78. Guttoff M, Saberi AH, Mcclements DJ. Formation of vitamin D nanoemulsion-based delivery systems by spontaneous emulsification: factors affecting particle size and stability. *Food Chem*. 2015;171:117–122. doi:10.1016/j.foodchem.2014.08.087
79. Ghadiri M, Fatemi S, Vatanara A, et al. Loading hydrophilic drug in solid lipid media as nanoparticles: statistical modeling of entrapment efficiency and particle size. *Int J Pharm*. 2012;424(1–2):128–137. doi:10.1016/j.ijpharm.2011.12.037
80. Mahmood S, Taher M, Mandal UK. Experimental design and optimization of raloxifene hydrochloride loaded nanotransfersomes for transdermal application. *Int J Nanomedicine*. 2014;9:4331–4346. doi:10.2147/IJN.S65408
81. Al-Mahallawi AM, Khowessah OM, Shoukri RA. Nano-transfersomal ciprofloxacin loaded vesicles for non-invasive trans-tympanic ototopical delivery: in-vitro optimization, ex-vivo permeation studies, and in-vivo assessment. *Int J Pharm*. 2014;472(1–2):304–314. doi:10.1016/j.ijpharm.2014.06.041
82. Zidan AS, Rahman Z, Khan MA. Product and process understanding of a novel pediatric anti-HIV tenofovir niosomes with a high-pressure homogenizer. *Eur J Pharm Sci*. 2011;44(1–2):93–102. doi:10.1016/j.ejps.2011.06.012
83. Severino P, Santana MHA, Souto EB. Optimizing SLN and NLC by 2 2 full factorial design: effect of homogenization technique. *Mater Sci Eng C*. 2012;32(6):1375–1379. doi:10.1016/j.msec.2012.04.017
84. Pandita D, Kumar S, Poonia N, Lather V. Solid lipid nanoparticles enhance oral bioavailability of resveratrol, a natural polyphenol. *Food Res Int*. 2014;62:1165–1174. doi:10.1016/j.foodres.2014.05.059
85. Cooper DL, Harirforoosh S. Effect of formulation variables on preparation of celecoxib loaded polylactide-co-glycolide nanoparticles. *PLoS One*. 2014;9(12):1–22. doi:10.1371/journal.pone.0113558
86. Gala RP, Khan I, Elhissi AMA, Alhnan MA. A comprehensive production method of self-cryoprotected nano-liposome powders. *Int J Pharm*. 2015;486(1–2):153–158. doi:10.1016/j.ijpharm.2015.03.038
87. Park JB, Noh Hg, Jung JH, et al. Enhanced transdermal delivery and optimization of nano-liposome preparation using hydrophilic drug. *Journal of Pharmaceutical Investigation*. 2012;42:57–63. doi:10.1007/s40005-012-0009-4
88. Malaria C, Schools E. Available online through. *JbsowebCom*. 2010;3(9):2280–2283.
89. Ahmed TA. Preparation of transfersomes encapsulating sildenafil aimed for transdermal drug delivery: plackett-Burman design and characterization. *J Liposome Res*. 2015;25(1):1–10. doi:10.3109/08982104.2014.950276
90. Salama HA, Mahmoud AA, Kamel AO, Abdel HM, Awad GAS. Brain delivery of olanzapine by intranasal administration of transfersomal vesicles. *J Liposome Res*. 2012;22(4):336–345. doi:10.3109/08982104.2012.700460
91. Zhang Y, Chen T, Yuan P, et al. Encapsulation of honokiol into self-assembled pectin nanoparticles for drug delivery to HepG2 cells. *Carbohydr Polym*. 2015;133:31–38. doi:10.1016/j.carbpol.2015.06.102
92. Xu C, Tang Y, Hu W, et al. Investigation of inclusion complex of honokiol with sulfobutyl ether-β-cyclodextrin. *Carbohydr Polym*. 2014;113:9–15. doi:10.1016/j.carbpol.2014.06.059
93. Aisha AFA, Majid AMSA, Ismail Z. Preparation and characterization of nano liposomes of Orthosiphon stamineus ethanolic extract in soybean phospholipids. *BMC Biotechnol*. 2014;14(1):1–11. doi:10.1186/1472-6750-14-23
94. Sun S, Liang N, Kawashima Y, Xia D, Cui F. Hydrophobic ion pairing of an insulin-sodium deoxycholate complex for oral delivery of insulin. *Int J Nanomedicine*. 2011;6:3049–3056. doi:10.2147/ijn.s26450
95. Bromma K, Bannister A, Kowalewski A, Cicon L, Chithrani DB. Elucidating the fate of nanoparticles among key cell components of the tumor microenvironment for promoting cancer nanotechnology. *Cancer Nanotechnol*. 2020;11(1):8. doi:10.1186/s12645-020-00064-6
96. Brownlee WJ, Seib FP. Impact of the hypoxic phenotype on the uptake and efflux of nanoparticles by human breast cancer cells. *Sci Rep*. 2018;8(1):12318. doi:10.1038/s41598-018-30517-3
97. Kou L, Sun J, Zhai Y, He Z. The endocytosis and intracellular fate of nanomedicines: implication for rational design. *Asian J Pharm Sci*. 2013;8(1):1–10. doi:10.1016/j.ajps.2013.07.001
98. Watanabe S, Boucrot E. Fast and ultrafast endocytosis. *Curr Opin Cell Biol*. 2017;47:64–71. doi:10.1016/j.ceb.2017.02.013
99. Wu W, Xue W. Evaluation of anticancer activity of honokiol by complexation with hydroxypropyl-β-cyclodextrin. *Colloids Surf B*. 2020;196:111298. doi:10.1016/j.colsurfb.2020.111298
100. Godugu C, Doddapaneni R, Singh M. Honokiol nanomicellar formulation produced increased oral bioavailability and anticancer effects in triple negative breast cancer (TNBC). *Colloids Surf B*. 2017;153:208–219. doi:10.1016/j.colsurfb.2017.01.038

101. Wang J, Yang H, Li Q, et al. Novel nanomicelles based on rebaudioside A: a potential nanoplatform for oral delivery of honokiol with enhanced oral bioavailability and antitumor activity. *Int J Pharm*. 2020;590:119899. doi:10.1016/j.ijpharm.2020.119899
102. Swidan SA, Hassan MM, Elmansy MN, Swidan SA. Synergistic therapeutic effect of nano-honokiol and 5-fluorouracil on the induced-tongue cancer in rats. *J Oral Maxillofac Surgery Med Pathol*. 2020;32(6):556–562. doi:10.1016/j.ajoms.2020.06.003
103. Zhu J, Xu S, Gao W, Feng J, Zhao G. Honokiol induces endoplasmic reticulum stress-mediated apoptosis in human lung cancer cells. *Life Sci*. 2019;221:204–211. doi:10.1016/j.lfs.2019.01.046
104. Lu CH, Chen SH, Chang YS, et al. Honokiol, a potential therapeutic agent, induces cell cycle arrest and program cell death in vitro and in vivo in human thyroid cancer cells. *Pharmacol Res*. 2017;115:288–298. doi:10.1016/j.phrs.2016.11.038
105. Lee JS, Sul JY, Park JB, Lee MS, Cha EY, Ko YB. Honokiol induces apoptosis and suppresses migration and invasion of ovarian carcinoma cells via AMPK/mTOR signaling pathway. *Int J Mol Med*. 2019;43(5):1969–1978. doi:10.3892/ijmm.2019.4122
106. Huang K, Chen Y, Zhang R, et al. Honokiol induces apoptosis and autophagy via the ROS/ERK1/2 signaling pathway in human osteosarcoma cells in vitro and in vivo article. *Cell Death Dis*. 2018;9(2):1–17. doi:10.1038/s41419-017-0166-5
107. Tansi FL, Fröbel F, Maduabuchi WO, et al. Effect of matrix-modulating enzymes on the cellular uptake of magnetic nanoparticles and on magnetic hyperthermia treatment of pancreatic cancer models in vivo. *Nanomater*. 2021;11(2). doi:10.3390/nano11020438
108. Iida J, McCarthy JB. Expression of collagenase-1 (MMP-1) promotes melanoma growth through the generation of active transforming growth factor-β. *Melanoma Res*. 2007;17(4):205–213. doi:10.1097/CMR.0b013e3282a660ad
109. Bhagyaraj E, Ahuja N, Kumar S, et al. TGF-β induced chemoresistance in liver cancer is modulated by xenobiotic nuclear receptor PXR. *Cell Cycle*. 2019;18(24):3589–3602. doi:10.1080/15384101.2019.1693120
110 Sebak A, El-Shenawy B, El-Safy S, El-Shazly M. From Passive Targeting to Personalized Nanomedicine: Multidimentional Insights on Nanoparticles' Interaction with the Tumor Microenvironment. *Curr Pharm Biotechnol*. 2020;21(15). doi:10.2174/1389201021666201211103856111.
111 Zhang S, Che D, Yang F, et al. Tumor-associated macrophages promote tumor metastasis via the TGF-β/SOX9 axis in non-small cell lung cancer. *Oncotarget*. 2017;8(59):99801–99815. doi:10.18632/oncotarget.21068
112. Steitz AM, Steffes A, Finkernagel F, et al. Tumor-associated macrophages promote ovarian cancer cell migration by secreting transforming growth factor beta induced (TGFBI) and tenascin C. *Cell Death Dis*. 2020;11(4):1–15. doi:10.1038/s41419-020-2438-8
113. Zonneville J, Safina A, Truskinovsky AM, Arteaga CL, Bakin AVTGF-B. signaling promotes tumor vasculature by enhancing the pericyte-endothelium association. *BMC Cancer*. 2018;18(1):670. doi:10.1186/s12885-018-4587-z
114. Wang Y, Jiang M, Li Z, et al. Hypoxia and TGF-β1 lead to endostatin resistance by cooperatively increasing cancer stem cells in A549 transplantation tumors. *Cell Biosci*. 2015;5(1):72. doi:10.1186/s13578-015-0064-4
115. Bellomo C, Caja L, Moustakas A. Transforming growth factor β as regulator of cancer stemness and metastasis. *Br J Cancer*. 2016;115(7):761–769. doi:10.1038/bjc.2016.255
116. You H, Ding W, Rountree CB. Epigenetic regulation of cancer stem cell marker CD133 by transforming growth factor-β. *Hepatology*. 2010;51(5):1635–1644. doi:10.1002/hep.23544
117. Mansour H, Elkhoda R, Anwar R, Habeeb MR, Mohammed MA. Regulation of cancer stem cell marker (CD133) by transforming growth factor beta in hepatocellular carcinoma. *Int J Cancer Res*. 2014;10(2):65–73. doi:10.3923/ijcr.2014.65.73
118. Müller L, Tunger A, Plesca I, et al. Bidirectional crosstalk between cancer stem cells and immune cell subsets. *Front Immunol*. 2020;11:140. doi:10.3389/fimmu.2020.00140
119. Liu SH, Lee WJ, Lai DW, et al. Honokiol confers immunogenicity by dictating calreticulin exposure, activating ER stress and inhibiting epithelial-to-mesenchymal transition. *Mol Oncol*. 2015;9(4):834–849. doi:10.1016/j.molonc.2014.12.009
120. Chao MP, Jaiswal S, Weissman-Tsukamoto R, et al. Calreticulin is the dominant pro-phagocytic signal on multiple human cancers and is counterbalanced by CD47. *Sci Transl Med*. 2010;2(63):63ra94. doi:10.1126/scitranslmed.3001375
121. Yuan J, Shi X, Chen C, et al. High expression of CD47 in triple negative breast cancer is associated with epithelial-mesenchymal transition and poor prognosis. *Oncol Lett*. 2019;18(3):3249–3255. doi:10.3892/ol.2019.10618
122. Fan Y, Xue W, Schachner M, Zhao W. Honokiol eliminates glioma/glioblastoma stem cell-like cells via JAK-STAT3 signaling and inhibits tumor progression by targeting epidermal growth factor receptor. *Cancers (Basel)*. 2019;11(5):1. doi:10.3390/cancers11010022
123. Yao CJ, Lai GM, Yeh CT, et al. Honokiol eliminates human oral cancer stem-like cells accompanied with suppression of Wnt/β-catenin signaling and apoptosis induction. *Evid Based Complement Altern Med*. 2013;2013:1–10. doi:10.1155/2013/146136
124. Lai I-C, Shih P-H, Yao C-J, et al. Elimination of cancer stem-like cells and potentiation of temozolomide sensitivity by honokiol in glioblastoma multiforme cells. *PLoS One*. 2015;10(3):e0114830. doi:10.1371/journal.pone.0114830
125. Tan W, Tang H, Jiang X, et al. Metformin mediates induction of miR-708 to inhibit self-renewal and chemoresistance of breast cancer stem cells through targeting CD47. *J Cell Mol Med*. 2019;23(9):5994–6004. doi:10.1111/jcmm.14462
126. Maehara O, Ohnishi S, Asano A, et al. Metformin regulates the expression of CD133 through the AMPK-CEBPβ pathway in hepatocellular carcinoma cell lines. *Neoplasia*. 2019;21(6):545–556. doi:10.1016/j.neo.2019.03.007
127. Chai X, Chu H, Yang X, Meng Y, Shi P, Gou S. Metformin increases sensitivity of pancreatic cancer cells to gemcitabine by reducing CD133+ cell populations and suppressing ERK/P70S6K signaling. *Sci Rep*. 2015;5(1):14404. doi:10.1038/srep14404
128. Gou S, Cui P, Li X, Shi P, Liu T, Wang C. Low concentrations of metformin selectively inhibit CD133+ cell proliferation in pancreatic cancer and have anticancer action. *PLoS One*. 2013;8(5):e63969. doi:10.1371/journal.pone.0063969
129. Das A, Datta S, Roche E, et al. Novel mechanisms of Collagenase Santyl Ointment (CSO) in wound macrophage polarization and resolution of wound inflammation. *Sci Rep*. 2018;8(1):1696. doi:10.1038/s41598-018-19879-w
130. Zhao M, Wang Y, Du C, Liu Y, Zhang N, Luo F. Aspirin and metformin exhibit antitumor activity in murine breast cancer. *Oncol Rep*. 2018;39(3):1414–1422. doi:10.3892/or.2018.6190